2005

The Scintillation Index In Moderate To Strong Turbulence For The Gaussian Beam Wave Along A Slant Path

Fredrick Eugene Thomas
University of Central Florida

THE SCINTILLATION INDEX IN MODERATE TO STRONG TURBULENCE FOR THE GAUSSIAN BEAM WAVE ALONG A SLANT PATH

by

FREDRICK E. THOMAS
B.S. University of Central Florida, 2003

A thesis submitted in partial fulfillment of the requirements
for the degree of Master of Science
in the Department of Mathematics
in the College of Arts and Sciences
at the University of Central Florida
Orlando, Florida

Summer Term
2005

ABSTRACT

Scintillation is one of the most common statistics in the literature of mathematical modeling of laser propagation through random media. One approach to estimating scintillation is through the Rytov approximation, which is limited to weak atmospheric turbulence. Recently, an improvement of the Rytov approximation was developed employing a linear filter function technique. This modifies the Rytov approximation and extends the validity into the moderate to strong regime. In this work, an expression governing scintillation of a Gaussian beam along an uplink slant path valid in all regimes of turbulence is presented, as well as results for the limiting cases of a plane wave and a spherical wave.

In the memory of my beloved father, Dalton Eugene Thomas

ACKNOWLEDGMENTS

First and foremost, I would like to express my deepest gratitude to my mentor, advisor, and committee chair, Dr. Cynthia Young. Her wisdom and utmost concern led me through the majority of my time at UCF. Without her guiding hand, neither this work nor my future scientific career would ever come to fruition. Also, I would like to extend my appreciation to Dr. Larry Andrews for selflessly weathering my numerous queries, and Dr. Xin Li for his advice and serving on my committee.

Finally, I must acknowledge the support of my friends and family. In particular, I want to show appreciation to my sister for being a pillar of strength and setting the example, and my mother for her everlasting and unconditional understanding and devotion.

TABLE OF CONTENTS

LIST OF FIGURES

CHAPTER 1: INTRODUCTION

Over the last several decades, interest in optical communication technology has flourished, particularly for satellite communication serving as links for ground-to-air/space and air/space-to-ground scenarios. Technical advancements in the field have renewed interest in the statistical modeling of atmospheric laser propagation phenomena. This interest stems from the inherent advantages optical wave systems have over conventional radio frequency systems. These include a potentially higher data transmission rate, smaller antennas, lower mass, volume, and power requirements, which are vital for battery-operated satellites, and more secure channels.

Unfortunately, while the chief reason for lasers' inherent advantages stem from having wavelengths of smaller magnitude than radio waves, it is also the chief reason for their disadvantages. Optical systems are much more susceptible to drops in channel visibility for a given threshold. In order to model visibility, weather patterns for the area of optical transmission are required. Both atmospheric parameters such as wind speed and temperature and topological issues, including geographic location and height, are required. Due to this, visibility and scintillation are expected to have a high degree of correlation.

As a wave propagates through the atmosphere, turbulent eddies cause deleterious effects, namely reduction in spatial coherence. In addition, intensity fluctuations (scintillation) and random changes in the beam direction (beam wandering) occur. Outside of inclement weather patterns such as rain and snow, scintillations associated with the signal at the receiver are primarily responsible for this deleterious effect [1, 2].

While there have been several models developed characterizing this phenomenon, they are valid only for weak fluctuations, which severely limits the path length and zenith angle (usually a maximum of 55-60 degrees). The new theory employed in this work is a tractable heuristic scintillation model, connecting the weak, moderate, and strong regimes of turbulence. This is accomplished by assuming that only turbulent eddies in the atmosphere that are smaller than the propagating wave's coherence radius or larger than the wave's scattering disk are chiefly responsible for scintillation. In effect, this new theory acts as a filter function, eliminating intermediate scale sizes that lose their ability to refract and diffract the beam. The scintillation model for a Gaussian beam wave propagating along a slant path incorporating this theory is presented for both on and off-axis cases.

CHAPTER 2: ATMOSPHERIC TURBULENCE

A combination of temperature and wind speed variations cause unstable air masses, which break up into turbulent eddies of varying sizes. The maximum size of these eddies is limited to the Reynolds number, a non-dimensional ratio of inertial force to viscous force. This maximum size, which is usually on the order of one to one hundred meters, is known as the outer scale L_0. Due to inertial forces, these eddies will continually break down until reaching a minimum size on the order of millimeters, known as the inner scale l_0. After these eddies reach this minimum size, they dissipate into heat. The eddies attenuate and redirect the energy of a propagating laser beam based on the relative size of the wave front in relation to l_0 and L_0. The index of refraction fluctuations are referred to as optical turbulence [1].

Since these fluctuations are random, spatial statistical quantities are used to describe the atmosphere and the optical wave behavior. Air's index of refraction, $n(\mathbf{R}) = 1 + n_1(\mathbf{R})$, where n_1 is a minute random value with a zero average value. If we want to compare the index of refractions at two different points in space, we use the covariance function,

$$B_n(\mathbf{R}_1, \mathbf{R}_2) = \langle n_1(\mathbf{R}_1) n_1(\mathbf{R}_2) \rangle \tag{1}$$

where <> signify an ensemble, or long-term, average. Assuming the atmosphere is statistically homogenous and isotropic, (1) only depends on the magnitude R of vector $\mathbf{R} = \mathbf{R}_1 + \mathbf{R}_2$. Therefore, (1) becomes

$$B_n(R) = \langle n_1(\mathbf{R}_1 + \mathbf{R}) n_1(\mathbf{R}_1) \rangle . \tag{2}$$

We use the power spectral density function of the index of refraction, $\Phi_n(\kappa)$, to describe the atmosphere's turbulent energy, where κ is the scalar spatial wave number. It is defined by a three-dimensional Fourier transform of covariance function (2). Assuming the random field is also subject to both statistical homogeneity and isotropy constraints, we can reduce $\Phi_n(\kappa)$ to

$$\Phi_n(\kappa) = \frac{1}{2\pi^2\kappa}\int_0^\infty B_n(R)R\sin(\kappa R)dR\,. \tag{3}$$

Equation (3) characterizes atmospheric turbulence. There are multiple spectral models available, with one of the earliest being the Kolmogorov spectrum, defined as

$$\Phi_n(\kappa) = 0.033C_n^2\kappa^{11/3}\,, \tag{4}$$

where C_n^2 is the index of refraction structure parameter, describing index of refraction fluctuation strength, which is related to turbulence strength [1]. Values range from 10^{-17} to 10^{-12} $m^{-2/3}$ for weak to strong turbulence respectively. This model fails to incorporate the effects of inner or outer scales, which can play a significant role in modeling scintillation. The Tatarskii spectrum model, which includes inner scale only, is defined as

$$\Phi_n(\kappa) = 0.033C_n^2\kappa^{11/3}\exp\left(-\frac{\kappa^2}{\kappa_m^2}\right), \quad \kappa >> \frac{1}{L_0}\,, \tag{5}$$

where $\kappa_m = 5.92/l_0$ [1]. Unlike the Kolmogorov spectrum, which treats eddy sizes on a continuous scale from zero to infinity, the Tatarskii spectrum incorporates a lower limit. Therefore, this model is finite and isotropic for wave numbers less than $1/L_0$. A spectral model that incorporates both inner and outer scale is the von Karman spectrum,

$$\Phi_n(\kappa) = \frac{0.033C_n^2}{\left(\kappa^2+\kappa_0^2\right)^{11/6}}\exp\left(-\frac{\kappa^2}{\kappa_m^2}\right), \tag{6}$$

where $\kappa_m = 1/l_0$ and $\kappa_0 = 2\pi/L_0$ [1].

CHAPTER 3: GAUSSIAN BEAM TURBULENCE AND PARAMETERS

Theoretical studies for optical wave propagation are usually designated as being part of a weak or strong fluctuation theory based on the value of the Rytov variance, which is defined as

$$\sigma_1^2 = 1.23 C_n^2 k^{7/6} L^{11/6}, \tag{7}$$

where L is the propagation path length and the optical wave number $k = 2\pi/\lambda$, with λ being wavelength. The Rytov variance is the scintillation index calculated for a plane wave using the Kolmogorov spectrum. Weak fluctuations correspond to a Rytov variance much less than unity, $\sigma_1^2 << 1$. Strong fluctuations, also known as the saturation regime, correspond to values of the Rytov variance much greater than unity, $\sigma_1^2 >> 1$. Moderate fluctuations are designated as $\sigma_1^2 \sim 1$. For a Gaussian beam, the Rytov variance as given is not an adequate descriptor. Since weak fluctuations correspond to the entire beam profile being less than unity, we strengthen the conditions to [1]

$$\sigma_1^2 < 1 \quad and \quad \sigma_1^2 \Lambda_1^{5/6} < 1, \tag{8}$$

where $\Lambda_1 = 2L/kW^2$, with W being the beam radius in free space at the receiver. If either condition in (8) is violated, the fluctuations are considered to be moderate or strong.

In general, laser beams and optical waves are represented by one of three models: an infinite plane wave, a spherical wave, or the Gaussian beam wave. Like any electromagnetic wave, a propagating laser beam obeys the wave equation derived from Maxwell's equations. For simplicity, we use the time-independent reduced wave equation

$$\nabla^2 U_0 + k^2 U_0 = 0, \tag{9}$$

where ∇^2 is the Laplacian, and U_0 is the complex field amplitude at the transmitter [1]. Assuming time variations in the field are sinusoidal in nature, we look for solutions of the field in the following form

$$U(\mathbf{R},t) = U_0(\mathbf{R})e^{-i\omega t}, \tag{10}$$

where ω is the angular frequency. Note that the field, U, is a function of space, $\boldsymbol{R} = (x, y, z)$ [1]. We assume that propagation along the z-axis is much greater than transverse spreading of the wave, letting us to write U_0 as

$$U_0(r,z) = V(r,z)e^{ikz}, \tag{11}$$

where r is the scalar distance perpendicular to the direction of propagation and $r^2 = x^2 + y^2$. This reduces (9) to the parabolic wave equation,

$$\frac{1}{r}\frac{\partial}{\partial r}\left(\frac{1}{r}\frac{\partial V}{\partial r}\right) + 2ik\left(\frac{\partial V}{\partial z}\right) = 0. \tag{12}$$

In the case of a plane wave, U_0 takes the form of

$$U_0(r,z) = A_0 e^{i\Phi_0 + ikz}, \tag{13}$$

where A_0 and Φ_0 are amplitude and phase constants, respectively. Note how only phase changes while propagating since amplitude is independent of z. For a spherical wave, the complex amplitude is given by

$$U_0(r,0) = \lim_{r\to 0}\frac{e^{ikr}}{4\pi r}. \tag{14}$$

Note that both (13) and (14) do not naturally occur, but are mathematical limits used in certain scenarios instead of a Gaussian beam profile due to their simplicity. As it propagates along z, the spherical wave is approximated by [1]

$$U_0(r,z) \cong \frac{1}{4\pi z}\exp\left[ikz + \frac{ikr^2}{2z}\right]. \tag{15}$$

The plane wave model is not realistic since laser beams are not infinitely long, nor have constant amplitude. The spherical wave model suffers from the assumption that the laser beam starts from a point source. Thus, we come to the most accurate of the three models, the Gaussian beam wave, which is finite and has its intensity profile at its highest on-axis, and drops off the farther you look off-axis. The lowest-order Gaussian-beam at the transmitter, $z = 0$, is described by

$$U_0(r,0) = a_0 \exp\left(-\frac{r^2}{W_0^2} - i\frac{kr^2}{2F_0}\right), \tag{16}$$

where a_0 is constant amplitude, F_0 is the phase front radius of curvature and W_0 is the Gaussian beam radius at the transmitter. By using the paraxial approximation, (16) at a given distance $z = L$ in free space is described by

$$U_0(r,z) = a_0 \frac{W_0}{W}\exp\left(ikL - i\varphi - \frac{r^2}{W^2} - i\frac{kr^2}{2F^2}\right), \tag{17}$$

where W is the Gaussian beam radius at the receiver, F is the Gaussian beam phase front radius of curvature at the receiver, and φ is the longitudinal phase shift.

Since the plane wave model is infinitely long and the spherical wave model emanates from a point source, they can be described more simply. The Gaussian beam model, being finite, uses

extra non-dimensional parameters to describe the optical field at the transmitter and receiver. The transmitter curvature parameter, θ_0, and the transmitter Fresnel ratio, Λ_0, are defined by

$$\Theta_0 = 1 - \frac{L}{F_0}, \quad \Lambda_0 = \frac{2L}{kW_0^2}. \tag{18}$$

If $\Theta_0 < 1$, the beam is considered to be convergent, $\Theta_0 = 1$ denotes a collimated beam, and $\Theta_0 > 1$ marks a divergent beam [1].

The receiver beam parameters are governed by

$$\frac{1}{p(z)} = \frac{1}{\Theta_0 + i\Lambda_0} = \Theta - i\Lambda, \tag{19}$$

where Θ and Λ are

$$\Theta = \frac{\Theta_0}{\Theta_0^2 + \Lambda_0^2} = 1 + \frac{z}{F}, \quad \Lambda = \frac{\Lambda_0}{\Theta_0^2 + \Lambda_0^2} = \frac{2z}{kW^2}, \tag{20}$$

where W is the beam spot radius at the receiver and F is the phase front radius of curvature. When both Θ and Λ are zero, the Gaussian beam model reduces to a plane wave. When $\Theta = 1$ and $\Lambda = 0$, it reduces to the spherical wave. W and F are defined as [1]

$$W = \frac{W_0}{\sqrt{\Theta^2 + \Lambda^2}} = W_0\sqrt{\Theta_0^2 + \Lambda_0^2}, \quad F = \frac{F_0\left(\Theta^2 + \Lambda^2 - \Theta\right)}{(\Theta - 1)\left(\Theta^2 + \Lambda^2\right)}. \tag{21}$$

The mean intensity at the receiver is given by

$$I(r, L) = \frac{1}{\Theta_0^2 + \Lambda_0^2}\exp\left(-\frac{2r^2}{W^2}\right) = \left(\Theta^2 + \Lambda^2\right)\exp\left(-\frac{2r^2}{W^2}\right). \tag{22}$$

CHAPTER 4: BEAM STATISTICS AND MODULATION

With the given background on the Gaussian beam model, we can discuss the statistics that lead up to the scintillation index. For an optical wave, we study the mean, the beam's second moment of intensity, degree of coherence (DOC), and the mutual coherence function (MCF). The MCF is a generalized second moment of the optical field defined by

$$\Gamma(\mathbf{r}_1, \mathbf{r}_2, L) = \left\langle U(\mathbf{r}_1, L) U^*(\mathbf{r}_2, L) \right\rangle, \tag{23}$$

where (23) refers to the complex conjugate, and $\mathbf{r}_1$ and $\mathbf{r}_2$ are two vectors in the transverse plane to the propagation path. The MCF dictates the mean intensity, $\left\langle I(\mathbf{r}_1, L) \right\rangle$, which determines beam spreading due to atmospheric turbulence, and the complex degree of coherence, $\mathrm{DOC}(\mathbf{r}_1, \mathbf{r}_2, L)$, which describes coherence loss due to atmospheric turbulence [1].

Fluctuations in field irradiance is governed by the fourth-order moment of the field, given as

$$\Gamma_4(\mathbf{r}_1, \mathbf{r}_2, \mathbf{r}_3, \mathbf{r}_4, L) = \left\langle U(\mathbf{r}_1, L) U^*(\mathbf{r}_2, L) U(\mathbf{r}_3, L) U^*(\mathbf{r}_4, L) \right\rangle. \tag{24}$$

From this moment, we yield the second moment of irradiance, $\left\langle I^2(\mathbf{r}_1, L) \right\rangle$, which along with the mean irradiance defines the scintillation index, given as

$$\sigma_I^2(\mathbf{r}, L) = \frac{\left\langle I^2 \right\rangle - \left\langle I \right\rangle^2}{\left\langle I \right\rangle^2}. \tag{25}$$

Recall that the Rytov variance (7) is the scintillation index for an unbounded plane wave using the Kolmogorov spectrum. We assume that the field irradiance can be expressed as $I = xy$, where

x represents large-scale (refraction properties) and y denotes small-scale (diffraction properties) fluctuations. By assuming both of these fluctuations are statistically independent from each other and that equation (24) is unity, (24) takes the following form

$$\sigma_I^2(\mathbf{r},L) = \left\langle x^2 \right\rangle \left\langle y^2 \right\rangle - 1 = \left(1+\sigma_x^2\right)\left(1+\sigma_y^2\right) - 1 = \sigma_x^2 + \sigma_y^2 + \sigma_x^2\sigma_y^2, \tag{26}$$

where σ_x^2 and σ_y^2 are the respective variances of x and y [3]. Expressing these variances in terms of log-radiance allows us to rewrite them as

$$\sigma_I^2\left(\mathbf{r},L\right) = \exp\left(\sigma_{\ln x}^2 + \sigma_{\ln y}^2\right) - 1. \tag{27}$$

The correlation length of the intensity fluctuations causes small-scale scintillation, while refractive eddies on the order of the scattering disk cause large-scale scintillation [3]. The scattering disk is defined by the refractive cell size l, where the focusing angle, $\theta_F \sim l/L$, is equal to the average diffraction angle, θ_d. In weak fluctuations, θ_d is on the order of the square root of $1/kL$, and $1/\ k\rho_0$ in strong fluctuations. Therefore, $L/k\rho_0$ defines the scattering disk in strong fluctuations, where ρ_0 is the spatial coherence radius [3]. Figure 1 exhibits this filtering phenomenon in the plane wave case, where the shaded region denotes scale sizes that do not contribute to scintillation for a typical scenario [6]. Note that the gap widens as turbulence increases from the weak to strong regimes, as the coherence radius and scattering disk act as the minimum upper and lower values where scale sizes affect scintillation. The behavior is the same in both the spherical and Gaussian beam cases.

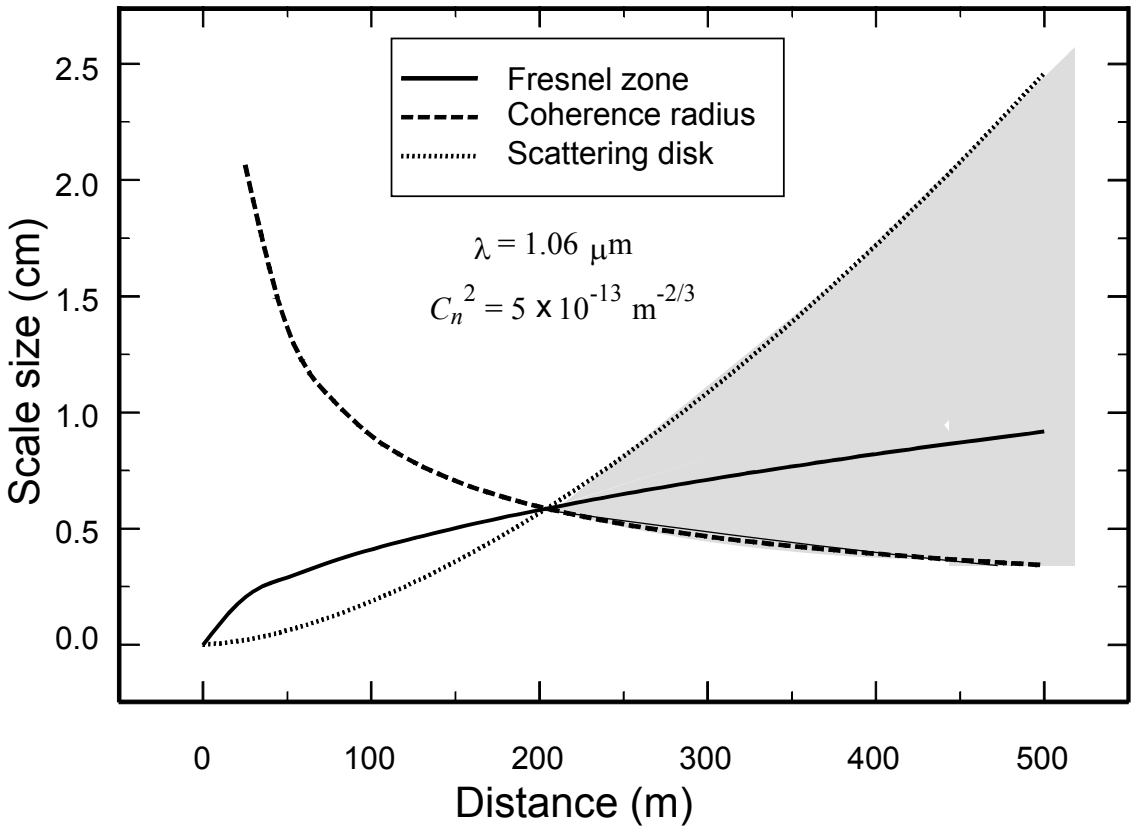

Figure 1: Scale sizes versus propagation distance for a plane wave.

With the physical reasoning behind the filter function approach set, an overview of its derivation follows.

4.1 Spatial Filter Function: Constant C_n^2

The spatial filter function approach will act as a modification to the standard Kolmogorov spectrum, presented in (7). The constant C_n^2 comes from assuming index-of-refractions are constant throughout the propagation path. The largest and smallest eddy sizes that affect the optical beam will act as cutoffs and are incorporated into the spectrum as a multiplicative filter. These are the outer scale and inner scale of turbulence, L_0 and l_0 respectively. One can consider

these values to be set to infinity and zero in the standard Kolmogorov spectrum. The *effective* Kolmogorov spectrum is given by

$$\Phi_n(\kappa,z) = 0.033C_n^2(z)\kappa^{-11/3}G(\kappa,z), \tag{28}$$

where G is the spatial filter and z is the propagation distance that varies from 0 (transmitter) to L (receiver) [1]. Note that this is only a filter being applied, and not a fundamental change of the Kolmogorov spectrum itself. In this case, the following can approximate G

$$G(\kappa,z) \approx G_x(\kappa) + G_y(\kappa) = \exp\left(-\frac{\kappa^2}{\kappa_x^2}\right) + \frac{\kappa^{11/3}}{\left(\kappa^2+\kappa_x^2\right)^{11/6}}. \tag{29}$$

Inner and outer scale effects are independent from propagation path, z. $G_x(\kappa)$ is the large-scale filter function with κ_x being the large-scale spatial-frequency cutoff, and $G_y(\kappa)$ and κ_y are the small-scale equivalents [1]. Since the only essential criteria for the functional form of (28) is that it provides a smooth transition between the known results of the weak and saturated regimes, the only other factor considered is mathematical convenience. G forces only spatial frequencies less than κ_x and greater than κ_y to pass. The frequency cutoffs are governed by the aforementioned coherence length and scattering disk, which leads to their general behavior patterns, denoted by the following [4]

$$\frac{L}{kl_x} = \frac{1}{\kappa_x} \sim \begin{cases} \sqrt{\dfrac{L}{k}}, & \dfrac{L}{k\rho_0^2} << 1 \\ \dfrac{L}{k\rho_0}, & \dfrac{L}{k\rho_0^2} >> 1 \end{cases} \tag{30}$$

$$l_y = \frac{1}{\kappa_y} \sim \begin{cases} \sqrt{\frac{L}{k}}, & \frac{L}{k\rho_0^2} << 1 \\ \rho_0, & \frac{L}{k\rho_0^2} >> 1 \end{cases}. \tag{31}$$

4.2 Spatial Filter Function: Variable C_n^2

By extending the propagation path the optical beam travels from strictly horizontal to slant and vertical paths, C_n^2 becomes dependent on altitude, h. One of the most common models that incorporates altitude is the Hufnagel-Valley (HV) model,

$$C_n^2(h) = 0.00594\left(\frac{v}{27}\right)^2 \left(10^{-5}h\right)^{10} \exp\left(-\frac{h}{1000}\right) + 2.7\times10^{-16} \exp\left(-\frac{h}{1500}\right) + A\exp\left(-\frac{h}{100}\right), \tag{32}$$

where v is the root-mean-square wind speed in meters per second (m/s), h is in meters (m) and A is the ground-level value of C_n^2 in meters-2/3 (m-2/3). In this document, v = 21 m/s, H is the satellite's height, h_0 is the height above ground of the lower transmitter/receiver, z is the zenith angle, and L, the total propagation distance, expands to $L = (H - h_0)$ sec z [4]. For all presented cases, a geostationary Earth orbit scenario is assumed, with H = 38,5000 km.

The filter function (28) is

$$\begin{aligned} G(\kappa, z; H, h_0) &= G_x(\kappa, z; H, h_0) + G_y(\kappa, z; H, h_0) \\ &= A(H, h_0)\exp\left\{-\int_0^1 D\left[\frac{\kappa\rho_0}{\kappa_x} w(\tau, z)\right] d\tau\right\}, \\ &+ \frac{B(H, h_0)\kappa^{11/3}}{\left(\kappa^2 + \kappa_y^2\right)^{11/6}} \end{aligned} \tag{33}$$

where A and B are weighting constants that account for $C_n^2(h)$'s variations in altitude on small and large-scale scintillations. D is the plane wave structure function, which is defined by

$$D(\rho) = 2.914k^2\rho^{5/3}\sec\zeta\int_{h_0}^{H} C_n^2(h)\,dh = 2.914\mu_0 k^2\rho^{5/3}\sec\zeta = 2\left(\frac{\rho}{\rho_0}\right)^{5/3}, \tag{34}$$

where μ_0 is defined by

$$\mu_0 = \int_{h_0}^{H} C_n^2(h)\,dh. \tag{35}$$

w in (32) is given by

$$w(\tau,z) = \begin{cases} \tau\left(1-\dfrac{\overline{\Theta}z}{L}\right) & \tau < \dfrac{z}{L} \\ \dfrac{z}{L}\left(1-\overline{\Theta}\tau\right) & \tau > \dfrac{z}{L} \end{cases}. \tag{36}$$

The large-scale filter function in (32) accounts for the phenomenon of large-scale scintillation is most prevalent near the transmitter. Furthermore, it is consistent with the results of the low-pass filter function in asymptotic theory [5]. This occurs when the weighting constant, A, reduces to unity when (31) is taken to the limiting case of a constant. The small-scale filter function is chiefly dependent on small eddies located near the receiver in strong fluctuations, and has little dependence to propagation distance, z. Assuming this is also valid for weak fluctuations, the weighting constant, B, also reduces to unity under the same condition.

In order to find A so that it reduces to unity with constant C_n^2, we calculate the scintillation index in the saturation regime,

$$\sigma_I^2(L) = 1 + 32\pi^2k^2\int_0^L\int_0^\infty \kappa\Phi_n(\kappa)G_x(\kappa,z;L,0)\sin\left[\frac{\kappa^2}{2k}w(z,z)\right]d\kappa dz, \tag{37}$$

where G_x in this case is

$$G_x(\kappa, z; L, 0) = \exp\left\{-\int_0^1 D\left[\frac{L\kappa}{k} w(\tau, z)\right] d\tau\right\}. \tag{38}$$

With the background behind the nature of turbulence and the new theory, the derivation of the scintillation index for standard and *effective* Kolmogorov spectrums in both horizontal slant paths is presented. This is performed for the unbounded plane wave, a spherical wave, and Gaussian beam wave models. Due to its simplicity, the plane wave case is shown first. A general flowchart is presented in Figure 2, with weak and strong referring to the standard and *effective* spectrums respectively. It is important to stress that due to the *effective* spectrum's tractability, one can recover all three cases from the *effective* slant case.

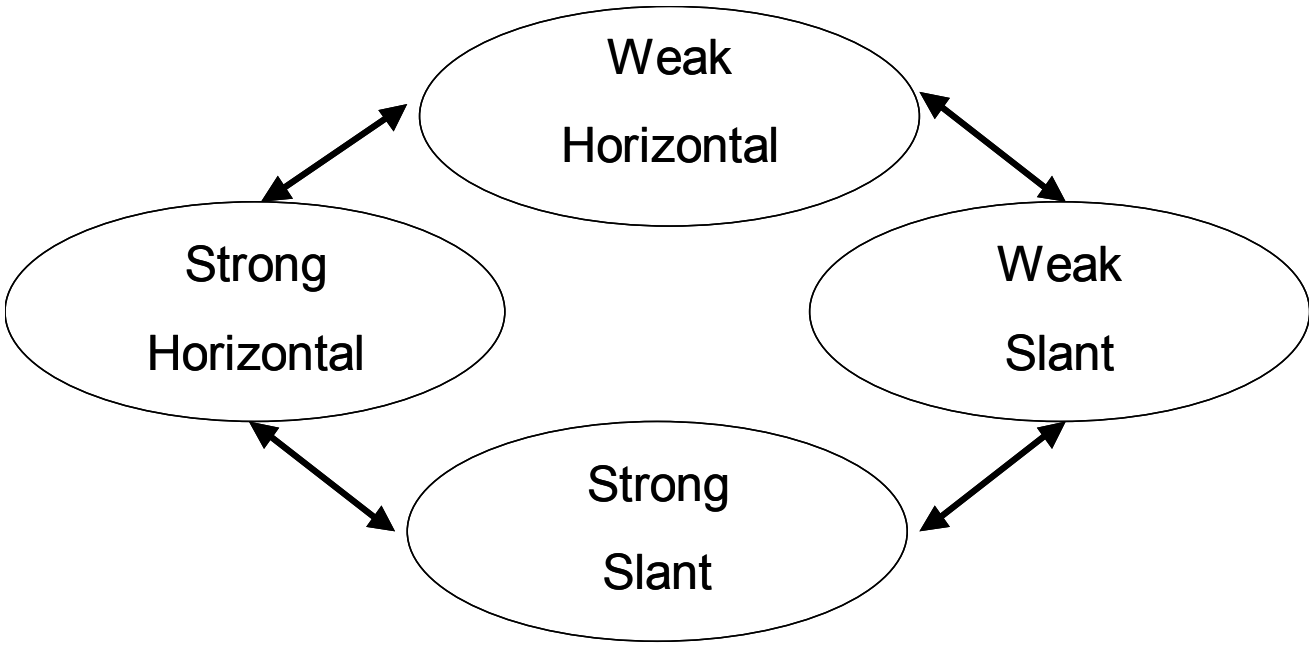

Figure 2: Flowchart for deriving each scintillation index case.

CHAPTER 5: SCINTILLATION INDEX - PLANE WAVE

The following section gives an overview for deriving the four scintillation index cases described in Figure 2 for an unbounded plane wave. Since the logarithm of the beam amplitude in the weak fluctuation regime is dominated by Gaussian statistics, early studies focused on log-amplitude variance instead of irradiance variance. A relation between an optical wave's log amplitude and complex phase perturbations altered by the atmosphere, ψ, is given by [1]

$$\chi(\mathbf{r},L)=\frac{1}{2}\left[\psi(\mathbf{r},L)+\psi^{*}(\mathbf{r},L)\right], \tag{39}$$

where

$$\psi(\mathbf{r},L)=\psi_1(\mathbf{r},L)+\psi_2(\mathbf{r},L). \tag{40}$$

The subscripts denote the first-order and second-order perturbations; no higher order terms are retained. The log-amplitude variance is defined by

$$\begin{aligned}\sigma_\chi^2(\mathbf{r},L)&=\left\langle\chi^2(\mathbf{r},L)\right\rangle-\left\langle\chi(\mathbf{r},L)\right\rangle^2\\&=\frac{1}{2}\mathrm{Re}\left[\left\langle\psi_1(\mathbf{r},L)\psi_1^{*}(\mathbf{r},L)\right\rangle+\left\langle\psi_1(\mathbf{r},L)\psi_1(\mathbf{r},L)\right\rangle\right],\\&=\frac{1}{2}\mathrm{Re}\left[E_2(\mathbf{r},\mathbf{r})+E_3(\mathbf{r},\mathbf{r})\right]\end{aligned} \tag{41}$$

where E_2 and E_3 are shorthand for the complex phase perturbation terms. Assuming that the turbulence is homogenous and isotropic, the log-amplitude variance of a Gaussian beam wave is defined as [1]

$$\begin{aligned}\sigma_\chi^2(\mathbf{r},L)=2\pi^2k^2L\int_0^1\int_0^\infty&\kappa\Phi_n(\kappa)e^{-\frac{\Lambda L\kappa^2\xi^2}{k}}\\&\times\left\{I_0\left(2\Lambda r\kappa\xi\right)-\cos\left[\frac{L\kappa^2}{k}\xi\left(1-\bar{\Theta}\xi\right)\right]\right\}d\kappa d\xi\end{aligned}, \tag{42}$$

where I_0 is the modified Bessel function and $\xi = 1 - z/L$ is a normalized distance variable. The scintillation index is defined in terms of the log-amplitude variance. When the log-amplitude variance is under weak fluctuations, the scintillation index is given as

$$\begin{aligned}\sigma_I^2(\mathbf{r},L) &= \exp\left[4\sigma_\chi^2(\mathbf{r},L)-1\right] \\ &\approx 4\sigma_\chi^2(\mathbf{r},L) \\ &= 8\pi^2k^2L\int_0^1\int_0^\infty \kappa\Phi_n(\kappa)e^{-\frac{\Lambda L\kappa^2\xi^2}{k}} \\ &\times\left\{I_0(2\Lambda r\kappa\xi)-\cos\left[\frac{L\kappa^2}{k}\xi\left(1-\bar{\Theta}\xi\right)\right]\right\}d\kappa d\xi\end{aligned} \quad . \tag{43}$$

For the plane wave case ($\Theta = 1$, $\Lambda = 0$), the scintillation index reduces to

$$\sigma_I^2(\mathbf{r},L) = 8\pi^2k^2L\int_0^1\int_0^\infty \kappa\Phi_n(\kappa)\left\{1-\cos\left[\frac{L\kappa^2}{k}\xi\right]\right\}d\kappa d\xi\,, \tag{44}$$

where this is the form used in deriving the four cases.

5.1 Standard Kolmogorov, Horizontal Path

Although the results are for the Kolmogorov case, the von Karman spectrum (6) is used during derivation to circumvent the discontinuities present. The inner and outer scales are reduced to zero and infinity respectively to reduce back to Kolmogorov results. Start with (44) using the von Karman spectrum,

$$\sigma_I^2(\mathbf{r},L) = 2.6056C_n^2k^2L\int_0^1\int_0^\infty \kappa\frac{\exp\left[-\kappa^2/\kappa_m^2\right]}{\left(\kappa^2+\kappa_0^2\right)^{11/6}}\left\{1-\cos\left[\frac{L\kappa^2}{k}\xi\right]\right\}d\kappa d\xi\,. \tag{45}$$

Separate the index into two separate integrals, $I_1$and I_2,

$$\sigma_I^2\left(\mathbf{r},L\right)=2.6056C_n^2k^2L\left[I_1-I_2\right]$$
$$I_1=\int_0^1\int_0^\infty \kappa\frac{\exp\left[-\kappa^2/\kappa_m^2\right]}{\left(\kappa^2+\kappa_0^2\right)^{11/6}}d\kappa d\xi \quad . \tag{46}$$
$$I_2=\int_0^1\int_0^\infty \kappa\frac{\exp\left[-\kappa^2/\kappa_m^2\right]}{\left(\kappa^2+\kappa_0^2\right)^{11/6}}\cos\left[\frac{L\kappa^2}{k}\xi\right]d\kappa d\xi$$

I_1 is solved using a previously known result,

$$\int_0^\infty \kappa^{2\mu}\frac{\exp\left[-\kappa^2/\kappa_m^2\right]}{\left(\kappa^2+\kappa_0^2\right)^{11/6}}d\kappa=\frac{1}{2}\kappa_0^{2\mu-8/3}\Gamma\left(\mu+\frac{1}{2}\right)U\left(\mu+\frac{1}{2};\mu-\frac{1}{3};\frac{\kappa_0^2}{\kappa_m^2}\right). \tag{47}$$

By using a small argument approximation for the hypergeometric function [1], and letting the outer scale go to infinity I_1 yields

$$I_1=\frac{1}{2}\kappa_0^{-5/3}\frac{\Gamma\left(5/6\right)}{\Gamma\left(11/6\right)}=\frac{3}{5}\kappa_0^{-5/3}. \tag{48}$$

By rewriting the cosine term as an imaginary exponential and using (47) for I_2 yields

$$I_2=\mathrm{Re}\left[\frac{\kappa_0^{-5/3}}{2}\int_0^1 U\left(1;\frac{1}{6};\kappa_0^2\left(\frac{1}{\kappa_m^2}+\frac{iL}{k}\xi\right)\right)d\xi\right] \tag{49}$$

Using a small argument approximation on the hypergeometric function and allowing the outer scale to go to infinity yields

$$I_2 = \mathrm{Re}\left[\frac{\kappa_0^{-5/3}}{2}\left(\frac{6}{5}+\Gamma\left(-5/6\right)\kappa_0^{5/3}\left(\frac{iL}{k}\right)^{5/6}\int_0^1 \xi^{5/6}d\xi\right)\right]. \tag{50}$$

Simplifying (50) results in

$$I_2 = \frac{3}{5}\kappa_0^{-5/3} + \mathrm{Re}\left[\Gamma\left(-5/6\right)\frac{6}{11}\left(\frac{iL}{k}\right)^{5/6}\right] = \frac{3}{5}\kappa_0^{-5/3} - .4715\left(\frac{L}{k}\right)^{5/6}. \tag{51}$$

Combining I_i and I_2 and inserting it into (46) yields

$$\begin{aligned}\sigma_I^2\left(\mathbf{r},L\right) &= 2.6056C_n^2k^2L\times.4715\left(\frac{L}{k}\right)^{5/6}\\ &= \sigma_1^2\end{aligned}, \tag{52}$$

which is the Rytov variance, the standard reference used for measuring strength of optical turbulence [1].

5.2 *Effective* Kolmogorov, Horizontal Path

Recall (26), which separated the large-scale and small-scale fluctuations in order to extend the scintillation index to strong fluctuations. By incorporating the spectrum defined by (28), the large-scale log-irradiance scintillation is given as

$$\sigma_{\ln x}^2 = 8\pi^2k^2\int_0^L\int_0^\infty \kappa\Phi_n\left(\kappa\right)G_x\left(\kappa\right)\left\{1-\cos\left[\frac{\kappa^2z}{k}\right]\right\}d\kappa dz, \tag{53}$$

while the small-scale scintillation is given as

$$\sigma_{\ln y}^2 = 8\pi^2 k^2 \int_0^L \int_0^\infty \kappa \Phi_n(\kappa) G_y(\kappa) \left\{ 1 - \cos\left[\frac{\kappa^2 z}{k} \right] \right\} d\kappa dz \,. \tag{54}$$

The derivation for (53) is performed first. Due to the strong fluctuations, a geometric optics approximation can be applied, limiting the approximation to the first two terms of the series expansion [1],

$$1 - \cos\left[\frac{\kappa^2 z}{k} \right] \cong \frac{1}{2} \left[\frac{\kappa^2 z}{k} \right]^2 . \tag{55}$$

Applying this approximation and noticing the integrals are separable, (53) becomes

$$\sigma_{\ln x}^2 = 1.303 C_n^2 k^2 \int_0^L z^2 dz \int_0^\infty \kappa^{4/3} \exp\left(-\frac{\kappa^2}{\kappa_x^2} \right) dk \tag{56}$$

Performing the rudimentary integrations results in

$$\sigma_{\ln x}^2 \approx 0.196 C_n^2 L^3 \left(\frac{\eta_x k}{L} \right)^{7/6} = 0.16 \sigma_1^2 \eta_x^{7/6}, \quad \eta_x << 1 \,, \tag{57}$$

where $\eta_x = L\kappa_x^2/k$, a non-dimensional spatial cutoff frequency parameter. Return to the small-scale case (54). Due to the small-scale being much greater than the Fresnel zone, the cosine term can be approximated by zero [2].

$$\sigma_{\ln y}^2 \approx 2.606 C_n^2 k^2 L \int_0^\infty \frac{\kappa d\kappa}{\left(\kappa^2 + \kappa_y^2 \right)^{11/6}} \tag{58}$$

By performing a change of variable and recognizing the integral form of the beta function, (58) leads to

$$\begin{aligned}\sigma_{\ln y}^2 &= \frac{2.606 C_n^2 k^2 L \kappa_y^{-5/3}}{2} \int_0^\infty \frac{\kappa d\kappa}{\left(\kappa^2 + \kappa_y^2\right)^{11/6}} \\ &= \frac{2.606 C_n^2 k^2 L \kappa_y^{-5/3}}{2} \frac{\Gamma(1)\Gamma(5/6)}{\Gamma(11/6)} = 1.563 C_n^2 k^2 L \kappa_y^{-5/3}\end{aligned}, \tag{59}$$

which simplifies to

$$\sigma_{\ln y}^2 = 1.563 C_n^2 k^{7/6} L^{11/6} \eta_y^{-5/6} = 1.27 \sigma_1^2 \eta_y^{-5/6}, \tag{60}$$

where $\eta_y = L\kappa_y^2/k$, a non-dimensional spatial cutoff frequency parameter. Now, the constants associated with the cutoffs need to be derived. Since the cutoffs relate to the small and large scale eddies, the following restrictions apply [3],

$$\eta_x = \begin{cases} \text{constant} & L/k\rho_0^2 << 1 \\ \sim k\rho_0^2 / L & L/k\rho_0^2 >> 1 \end{cases} \tag{61}$$

$$\eta_y = \begin{cases} \text{constant} & L/k\rho_0^2 << 1 \\ \sim L/k\rho_0^2 & L/k\rho_0^2 >> 1 \end{cases}. \tag{62}$$

Given this behavior, the cutoffs will assume the following forms, with four arbitrary constants related to the known weak and saturation regime results [3],

$$\eta_x = \frac{1}{c_1 + c_2 L/k\rho_0^2} \tag{63}$$

$$\eta_y = c_3 + c_4 \frac{L}{k\rho_0^2}. \tag{64}$$

As derived earlier, the scintillation index for weak fluctuations is given by the Rytov variance, σ_I^2. Knowing this, the scintillation index for the *effective* spectrum should reduce accordingly. Therefore,

$$\sigma_I^2 = \exp\left[\sigma_{\ln x}^2 + \sigma_{\ln y}^2\right] - 1 = \sigma_1^2 \,. \tag{65}$$

With this restriction, $c_1 = 3$ and $c_3 = 1/3$. It should be noted that while this leads back to the Rytov variance, it is not the only acceptable choice. In the saturation regime, large-scale scintillation should eventually vanish, creating the following restriction that $\sigma_{ln\,y}^{\;2} = \ln 2$ [3]. Therefore, $c_4 = 1.7$.

Finally, c_2 has to be set so that the scintillation index matches up with results in the saturation regime. Solving (36) for the plane wave case yields the following result [1],

$$\sigma_{I,saturation}^2 = 1 + \frac{0.86}{\sigma_1^{4/5}} = 1 + 0.92\left(\frac{k\rho_0^2}{L}\right)^{1/3}, \tag{66}$$

where the relation,

$$\frac{k\rho_0^2}{L} = 1.22\sigma_1^{5/3}, \tag{67}$$

was used. Matching (66) to the following relation of the *effective* scintillation index approaching the saturation regime, given by

$$\sigma_I^2 = \exp\left[\sigma_{\ln x}^2 + \sigma_{\ln y}^2\right] - 1 \approx \exp\left[2\sigma_{\ln x}^2\right] - 1 \approx 1 + \frac{0.24}{\sigma_1^{4/5}} c_2^{-7/6}, \tag{68}$$

yields $c_2 = 1/3$. Therefore, the non-dimensional cutoffs reduce to

$$\eta_x = \frac{2.61}{1+1.11\sigma_1^{12/5}} \tag{69}$$

$$\eta_y = 3\left(1+0.69\sigma_1^{12/5}\right). \tag{70}$$

Substituting these cutoffs into the large-scale and small-scale scintillation indices yields the scintillation index of a plane wave for the *effective* Kolmogorov spectrum along a horizontal path found in [2],

$$\begin{aligned}\sigma_I^2\left(L\right) &= \exp\left[\sigma_{\ln x}^2 + \sigma_{\ln y}^2\right] - 1 \\ &= \exp\left[\frac{0.49\sigma_1^2}{\left(1+1.11\sigma_1^{12/5}\right)^{7/6}} + \frac{0.51\sigma_1^2}{\left(1+0.69\sigma_1^{12/5}\right)^{5/6}}\right] - 1, \quad 0 \le \sigma_1^2 < \infty.\end{aligned} \tag{71}$$

Note that (71) is a ratio of the standard Kolmogorov result, reduces to the Rytov variance under the condition of weak fluctuations. Figure 2 presents a comparison between the standard and *effective* results, plotted against the Rytov variance. Note that in the weak regime, both cases match up well. It's only when turbulence strength reaches the moderate regime ($\sigma_I^2 \sim 1$) that the two results part ways. The weak case increases linearly without bound while the *effective* case makes a gradual decent back to unity from above.

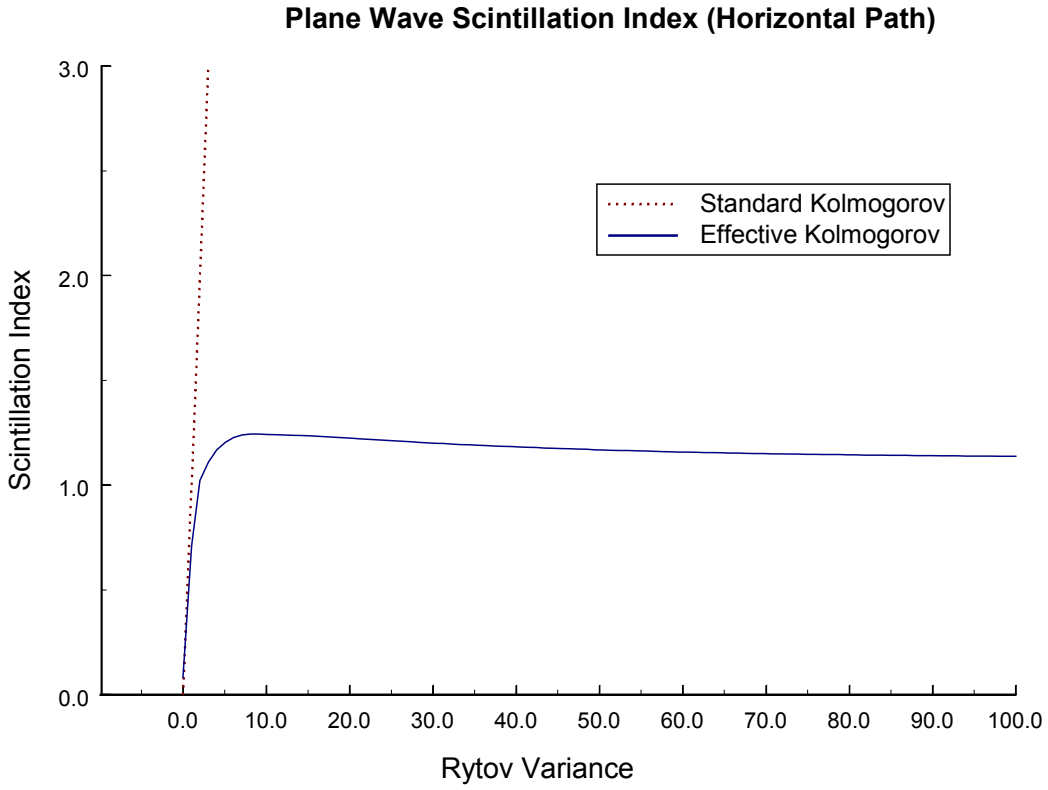

Figure 3: Comparison graph of weak (52) versus *effective* (71) plane wave results, based on Rytov Variance, σ_1^2.

5.3 Standard Kolmogorov, Slant Path

For this section, the standard Kolmogorov spectrum is used, but C_n^2 becomes dependent on altitude. As mentioned before, the HV model (32) is used. The scintillation index for a slant path is an important statistic for satellite communication systems. The plane wave case is used for the downlink scintillation index. Since the originating optical beam travels through space for the majority of the propagation path, space can be approximated as being a vacuum. By the time it reaches the Earth, the atmospheric effects are negligible, so the received beam is approximated by a plane wave. For a downlink scenario, normalized distance is defined as $\xi = (h - h_0)/(H -$

h_0), where h_0 is receiver height above ground level and H is the transmitter height above ground [1]. Also, due to the complexity of the HV model, the integrals along h are calculated numerically. The Kolmogorov spectrum in this case is defined by

$$\Phi_n(\kappa) = 0.033 C_n^2(h)\kappa^{11/3}. \tag{72}$$

Substituting for the slant path definition for propagation path, the scintillation index is defined as

$$\sigma_I^2 = 8\pi^2 k^2 \sec(\zeta) \int_{h_0}^{H}\int_{0}^{\infty} \kappa \Phi_n(h,\kappa)\left[1-\cos\left(\frac{L\kappa^2}{k}\xi\right)\right] d\kappa dh. \tag{73}$$

A similar method as in the weak horizontal case is used, where the von Karman spectrum is used for the derivation instead of the Kolmogorov spectrum. With that in mind, (73) becomes

$$\sigma_I^2 = 2.606 k^2 \sec(\zeta) \int_{h_0}^{H} C_n^2(h) \int_{0}^{\infty} \kappa \frac{\exp\left[-\kappa^2/\kappa_m^2\right]}{\left(\kappa^2+\kappa_0^2\right)^{11/6}}\left[1-\cos\left(\frac{L\kappa^2}{k}\xi\right)\right] d\kappa dh. \tag{74}$$

Using a similar method as in the weak horizontal case, (74) yields

$$\sigma_I^2 = 1.303 k^2 \kappa_0^{-5/3} \sec(\zeta) \int_{h_0}^{H} C_n^2(h) \times \operatorname{Re}\left[U\left(1;\frac{1}{6};\frac{\kappa_0^2}{\kappa_m^2}\right) - U\left(1;\frac{1}{6};\kappa_0^2\left(\frac{1}{\kappa_m^2}+\frac{iL}{k}\xi\right)\right)\right] dh. \tag{75}$$

Employing a small argument approximation on both hypergeometric functions transforms (75) into

$$\sigma_I^2 = 1.303k^2 \sec(\zeta) \int_{h_0}^{H} C_n^2(h)\Gamma(-1/6)\times$$
$$\operatorname{Re}\left[\left(\frac{1}{\kappa_m^2}\right)^{5/6} - \left(\left(\frac{1}{\kappa_m^2} + \frac{iL}{k}\xi\right)\right)^{5/6}\right] dh \quad (76)$$

By letting the outer scale cutoff go to infinity, (76) goes to

$$\sigma_I^2 = 8.825 \operatorname{Re}\left(i^{5/6}\right) k^{7/6} L^{5/6} \sec(\zeta) \int_{h_0}^{H} C_n^2(h)\xi^{5/6} dh . \quad (77)$$

Given that $L = (H - h_0)$ sec ζ, the downlink scintillation index, originally derived by Andrews and Phillips, is given by [2]

$$\sigma_I^2 = 2.25k^{7/6}\mu_1 \left(H - h_0\right)^{5/6} \sec^{11/6}(\zeta), \quad (78)$$

where μ_1 is defined as

$$\mu_1 = \int_{h_0}^{H} C_n^2(h)\left(\frac{h - h_0}{H - h_0}\right)^{5/6} dh . \quad (79)$$

The scintillation index reduces to the Rytov variance for a horizontal propagation path.

5.4 *Effective* Kolmogorov, Slant Path

For the *effective* spectrum along a slant path, the scintillation index given by (73) is still incorporated, but with the C_n^2 and filter function as defined in Section 4.2. Separating the scintillation index in terms of the small-scale and large-scale log-irradiance scintillation,

$$\sigma_{\ln y}^2 = 2.606B\left(H,h_0\right)k^2\sec\left(\zeta\right)\int_{h_0}^{H}C_n^2\left(h\right)\int_0^{\infty}\frac{\kappa}{\left(\kappa^2+\kappa_y^2\right)^{11/6}}\left\{1-\cos\left[\frac{L\kappa^2}{k}\xi\right]\right\}d\kappa dh \qquad (80)$$

$$\sigma_{\ln x}^2 = 2.606k^2\sec\left(\zeta\right)\int_{h_0}^{H}C_n^2\left(h\right)\int_0^{\infty}\kappa^{-8/3}G_x\left(\kappa,z;H,h_0\right)\left\{1-\cos\left[\frac{L\kappa^2}{k}\xi\right]\right\}d\kappa dh\,. \qquad (81)$$

Start with the small-scale term. Note that the kappa integration is equivalent to the *effective* horizontal case, where a small argument approximation and integral form of the beta function are used. Knowing this, (80) becomes

$$\sigma_{\ln y}^2 = 1.56B\left(H,h_0\right)\mu_0 k^{7/6}\left(H-h_0\right)^{5/6}\sec^{11/6}\left(\zeta\right)\eta_y^{5/6}\,, \qquad (82)$$

where μ_0 is defined as

$$\mu_0 = \int_{h_0}^{H}C_n^2\left(h\right)dh\,. \qquad (83)$$

By substituting for the weak slant scintillation index, (82) yields

$$\sigma_{\ln y}^2 = 0.7B\left(H,h_0\right)\left(\frac{\mu_0}{\mu_1}\right)\sigma_1^2\eta_y^{5/6}\,. \qquad (84)$$

To find the weighting constant, *B*, set (84) equal to the result found for small-scale scintillation in the *effective* horizontal case, (60). For tractability, *B* is found to be

$$B\left(H,h_0\right) = 1.83\frac{\mu_0}{\mu_1}\,. \qquad (85)$$

Return to the large-scale scintillation. Before it can be evaluated, the proper filter function has to be developed. For the plane wave case, the filter function is given as

$$
\begin{aligned}
G_x(\kappa,z) &= A(H,h_0)\exp\left\{-\int_0^1 D\left[\frac{\kappa\rho_0}{\kappa_x}w(\tau,z)\right]d\tau\right\} \\
&= A(H,h_0)\exp\left\{-2\left(\frac{\kappa}{\kappa_x}\right)^{5/3}\left[\int_0^{z/L}\tau^{5/3}d\tau+\int_{z/L}^1\left(\frac{z}{L}\right)^{5/3}d\tau\right]\right\} \\
&= A(H,h_0)\exp\left\{-2\left(\frac{\kappa}{\kappa_x}\right)^{5/3}\left[\frac{3}{8}\left(\frac{z}{L}\right)^{8/3}+\left(\frac{z}{L}\right)^{5/3}\left(1-\frac{z}{L}\right)\right]\right\}. \qquad (86) \\
&= A(H,h_0)\exp\left\{-2\left(\frac{\kappa}{\kappa_x}\right)^{5/3}\left(\frac{z}{L}\right)^{5/3}\left[\left(1-\frac{5}{8}\frac{z}{L}\right)\right]\right\} \\
&= A(H,h_0)\exp\left\{-2\left(\frac{\kappa}{\kappa_x}\right)^{5/3}\xi^{5/3}\left[\left(1-\frac{5}{8}\xi\right)\right]\right\}
\end{aligned}
$$

Incorporating the filter function and a geometrical optics approximation to the large-scale scintillation term, (81) reduces to

$$
\begin{aligned}
\sigma_{\ln x}^2 = 2.606A(H,h_0)(H-h_0)^2\sec^3(\zeta)\int_{h_0}^H C_n^2(h)\xi^2\times \\
\int_0^\infty \kappa^{5/3}\exp\left\{-2\left(\frac{\kappa}{\kappa_x}\right)^{5/3}\xi^{5/3}\left[\left(1-\frac{5}{8}\xi\right)\right]\right\}d\kappa dh \qquad (87)
\end{aligned}
$$

The kappa integration is the form of a gamma function, leading to

$$
\begin{aligned}
\sigma_{\ln x}^2 = .26A(H,h_0)(H-h_0)^2\kappa_x^{7/3}\sec^3(\zeta) \\
\int_{h_0}^H C_n^2(h)\left\{\xi^{-1/3}\left[1-\frac{5}{8}\xi\right]^{-7/5}\right\}dh \qquad (88)
\end{aligned}
$$

Denote the altitude-dependent integration with μ_2, along with the weak scintillation substitution, simplifying (88) to the following form

$$\begin{aligned}\sigma_{\ln x}^2 &= .26A\left(H,h_0\right)\mu_2\left(H-h_0\right)^{5/6}\sec^{11/6}\left(\zeta\right)\eta_x{}^{7/6} \\ &= .12A\left(H,h_0\right)\left(\frac{\mu_2}{\mu_1}\right)\sigma_1^2\eta_x{}^{7/6}\end{aligned}. \tag{89}$$

To find the weighting constant *A,* perform a similar requirement for the large-scale horizontal *effective* scintillation. This yields

$$A\left(H,h_0\right) = 4.68\frac{\mu_1}{\mu_2}. \tag{90}$$

Recall the cutoffs found during the *effective* horizontal case. With this information and the weighting constants, the scintillation of a plane wave for a slant path in all regimes of turbulence is given by

$$\begin{aligned}\sigma_I^2\left(L\right) &= \exp\left[\sigma_{\ln x}^2+\sigma_{\ln y}^2\right]-1 \\ &= \exp\left[\frac{0.49\sigma_1^2}{\left(1+1.11\sigma_1^{12/5}\right)^{7/6}}+\frac{0.51\sigma_1^2}{\left(1+0.69\sigma_1^{12/5}\right)^{5/6}}\right]-1, \quad 0\le\sigma_1^2<\infty\end{aligned}. \tag{91}$$

This matches the index originally derived by Andrews et. al. [2]. Notice that the form of (91) is equivalent to the form of (71), except that (91) incorporates the weak slant scintillation index. In Figure 4, a comparison between the standard and *effective* downlink scintillation is shown with varying zenith angle, which in turn varies fluctuation strength. As the angle becomes steeper,

causing the strength of atmospheric fluctuations to increase, the standard Kolmogorov case becomes unbounded. The effective Kolmogorov case converges to known saturation results.

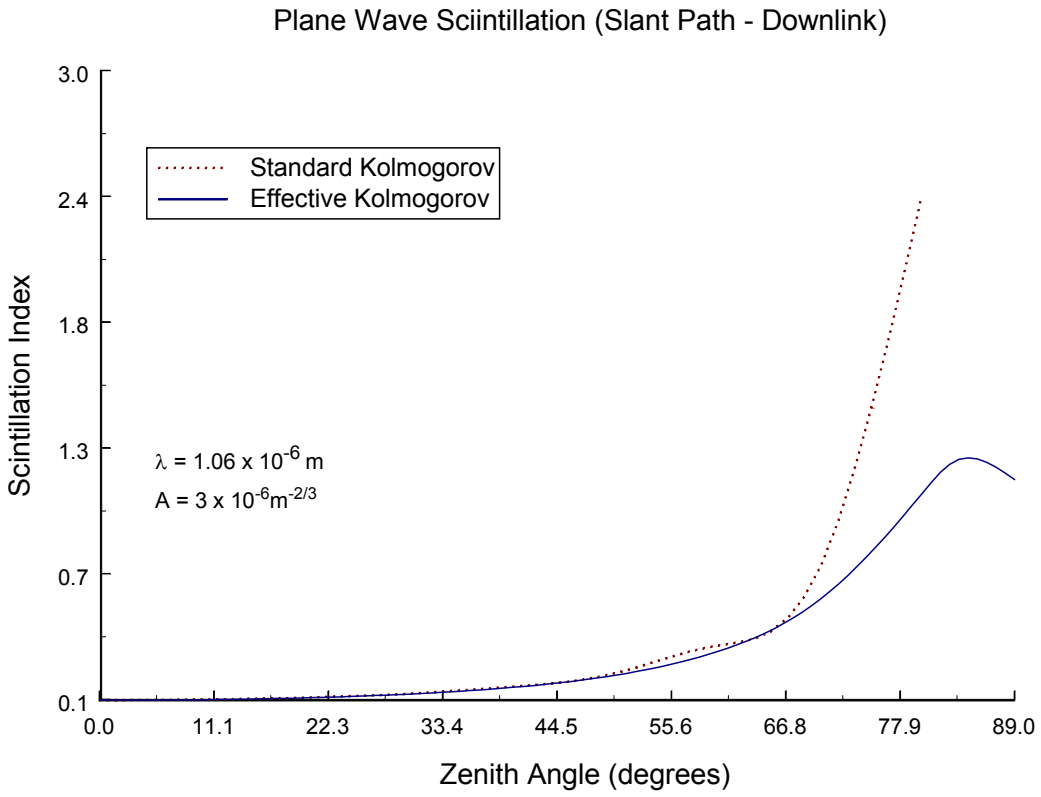

Figure 4: Comparison of weak (78) versus *effective* (91) plane wave scintillation for downlink path.

CHAPTER 6: SCINTILLATION INDEX - SPHERICAL WAVE

While the plane wave is primarily used for cases where propagation distance is extremely long and generally void of atmospheric turbulence (e.g., starlight, satellite communication originating from orbit), a spherical wave is used for cases where a small aperture receiver is located in or near a turbulent medium [1]. To imagine a spherical wave, consider the wave created by throwing a pebble into a still lake. Unlike the plane wave case where theta equals zero, theta equals one, $\Theta = 1$, for the spherical wave case. Lambda is still equal to one. This reduces the scintillation index equation given in (43) to

$$\sigma_I^2\left(\mathbf{r},L\right)=8\pi^2k^2L\int_0^1\int_0^\infty \kappa\Phi_n\left(\kappa\right)\left\{1-\cos\left[\frac{L\kappa^2}{k}\xi\left(1-\xi\right)\right]\right\}d\kappa d\xi\,, \tag{92}$$

which is similar to plane wave case, but leads to a more complicated cosine argument.

6.1 Standard Kolmogorov, Horizontal Path

Similar to the plane wave case, the von Karman spectrum (6) is used for calculating the index initially to take care of the discontinuities. Start with (92) using this spectrum, which yields

$$\sigma_I^2\left(\mathbf{r},L\right)=2.6056C_n^2k^2L\int_0^1\int_0^\infty \kappa\frac{\exp\left[-\kappa^2/\kappa_m^2\right]}{\left(\kappa^2+\kappa_0^2\right)^{11/6}}\left\{1-\cos\left[\frac{L\kappa^2}{k}\xi\left(1-\xi\right)\right]\right\}d\kappa d\xi\,. \tag{93}$$

Separate the index into two separate integrals, $I_1$and I_2

$$\sigma_I^2\left(\mathbf{r},L\right)=2.6056C_n^2k^2L\left[I_1-I_2\right]$$
$$I_1=\int_0^1\int_0^\infty \kappa\frac{\exp\left[-\kappa^2/\kappa_m^2\right]}{\left(\kappa^2+\kappa_0^2\right)^{11/6}}d\kappa d\xi \qquad (94)$$
$$I_2=\int_0^1\int_0^\infty \kappa\frac{\exp\left[-\kappa^2/\kappa_m^2\right]}{\left(\kappa^2+\kappa_0^2\right)^{11/6}}\cos\left[\frac{L\kappa^2}{k}\xi\left(1-\xi\right)\right]d\kappa d\xi$$

Note that I_1 is the same as in the plane wave case, which is equivalent to

$$I_1=\frac{1}{2}\kappa_0^{-5/3}\frac{\Gamma\left(5/6\right)}{\Gamma\left(11/6\right)}=\frac{3}{5}\kappa_0^{-5/3}. \qquad (95)$$

I_2 is solved in a similar manner. Rewrite the integral so that the cosine term is expressed as an imaginary exponential

$$I_2=\mathrm{Re}\left[\int_0^1\int_0^\infty \kappa\frac{\exp\left[-\kappa^2\left(\frac{1}{\kappa_m^2}+\frac{iL}{k}\xi\left(1-\xi\right)\right)\right]}{\left(\kappa^2+\kappa_0^2\right)^{11/6}}d\kappa d\xi\right]. \qquad (96)$$

Use the same integral formula (47) to yield

$$I_2=\mathrm{Re}\left[\frac{\kappa_0^{-5/3}}{2}\int_0^1 U\left(1;\frac{1}{6};\kappa_0^2\left(\frac{1}{\kappa_m^2}+\frac{iL}{k}\xi\left(1-\xi\right)\right)\right)d\xi\right]. \qquad (97)$$

Using a small argument approximation on the confluent hypergeometric, disregarding the small imaginary portion left, and letting the outer scale go to infinity yields

$$I_2 = \mathrm{Re}\left[\frac{\kappa_0^{-5/3}}{2}\left(\frac{6}{5}+\Gamma\left(-5/6\right)\kappa_0^{5/3}\left(\frac{iL}{k}\right)^{5/6}\int_0^1 \xi^{5/6}\left(1-\xi\right)^{5/6}d\xi\right)\right]. \qquad (98)$$

Note that the integration present is an alternate form of the beta function. The integral can be rewritten, simplifying (97),

$$I_2 = \mathrm{Re}\left[\frac{\kappa_0^{-5/3}}{2}\left(\frac{6}{5}+\frac{3\Gamma\left(-5/6\right)\Gamma\left(5/6\right)\Gamma\left(11/6\right)}{16\Gamma\left(-5/6\right)}\kappa_0^{5/3}\left(\frac{iL}{k}\right)^{5/6}\right)\right]. \qquad (99)$$

Simplifying the gamma functions yield

$$. \; I_2 = \frac{3}{5}\kappa_0^{-5/3} + \mathrm{Re}\left[.1\left(\frac{iL}{k}\right)^{5/6}\right]. \qquad (100)$$

By taking the real part of the complex term, I_2 is simplified to

$$. \; I_2 = \frac{3}{5}\kappa_0^{-5/3} + .1\left(\frac{L}{k}\right)^{5/6}\frac{\sqrt{3}-1}{2\sqrt{2}}. \qquad (101)$$

Combining I_1 and I_2 and placing them back into the scintillation index leads to

$$. \; \sigma_{I,l}^2\left(\mathbf{r},L\right) = 2.6056C_n^2k^2L\times.188\left(\frac{L}{k}\right)^{5/6} = .4\sigma_1^2, \qquad (102)$$

where the end result is merely a constant multiplier of the plane wave case, as shown by Andrews and Phillips [1].

6.2 *Effective* Kolmogorov, Horizontal Path

As one would expect, performing the integrations for the large-scale and small-scale scintillation indices is mostly trivial if the plane wave case has already been performed, especially due to the geometrical optics approximations used. The chief difference comes in the formulation of the spatial frequency cutoffs. The large-scale log-irradiance scintillation is given as

$$\sigma_{\ln x}^2 = 8\pi^2 k^2 \int_0^L \int_0^\infty \kappa \Phi_n(\kappa) G_x(\kappa) \left\{ 1 - \cos\left[\frac{\kappa^2 z}{k} \left(1 - \frac{z}{L} \right) \right] \right\} d\kappa dz \quad (103)$$

while the small-scale scintillation is given as

$$\sigma_{\ln y}^2 = 8\pi^2 k^2 \int_0^L \int_0^\infty \kappa \Phi_n(\kappa) G_y(\kappa) \left\{ 1 - \cos\left[\frac{\kappa^2 z}{k} \left(1 - \frac{z}{L} \right) \right] \right\} d\kappa dz \,. \quad (104)$$

Start with the large-scale scintillation. The only difference between (103) and (104) and their plane wave counterparts, (53) and (54) respectively, is the $(1 - z/L)$ term. As in the plane wave case, a geometric optics approximation is used due to the presence of only large-scale sizes

$$1 - \cos\left[\frac{\kappa^2 z}{k} \left(1 - \frac{z}{L} \right) \right] \cong \frac{1}{2} \left[\frac{\kappa^2 z}{k} \left(1 - \frac{z}{L} \right) \right]^2 . \quad (105)$$

Applying (105) yields two separable integrals,

$$\sigma_{\ln x}^2 = 1.303 C_n^2 \int_0^L z^2 \left(1 - z/L \right)^2 dz \int_0^\infty \kappa^{4/3} \exp\left(-\frac{\kappa^2}{\kappa_x^2} \right) dk \,. \quad (106)$$

Noting that the kappa integration is an alternate integral form of the gamma function, (106) simplifies to

$$\sigma_{\ln x}^2 = 0.0196 C_n^2 L^3 \left(\kappa_x^2\right)^{7/6} = 0.0196 C_n^2 L^3 \left(\frac{\eta_x k}{L}\right)^{7/6} = 0.016 \sigma_1^2 \eta_x^{7/6} . \quad (107)$$

One will notice that this result is merely a constant multiple difference from the plane wave result. For the small-scale case, the same approximation allowing the cosine term to be neglected that was used in the plane wave section applies here. This leads to an equivalent form found in the plane wave case. Therefore, the small-scale scintillation term has the following representation

$$\sigma_{\ln y}^2 = 1.27 \sigma_1^2 \eta_y^{-5/6} . \quad (108)$$

Now, the cutoffs must be found specifically for the spherical wave case. The same functional form is used,

$$\eta_x = \frac{1}{c_1 + c_2 L / k\rho_0^2} \quad (109)$$

$$\eta_y = c_3 + c_4 \frac{L}{k\rho_0^2} . \quad (110)$$

Match the *effective* scintillation index with the weak scintillation,

$$\sigma_I^2 = \exp\left[\sigma_{\ln x}^2 + \sigma_{\ln y}^2\right] - 1 = .4\sigma_1^2 . \quad (111)$$

As before, there is not a unique solution available, but the solution of $c_1 = 1/9$, $c_2 = 9$ is used. In the weak limit, this will reduce the scintillation index back to weak results. In strong fluctuations, large-scale scintillation should eventually vanish. Therefore, the following relation is used to find c_4,

$$\sigma_{\ln y}^2 = \ln 2 \quad \Rightarrow \quad c_4 = 1.7 \,. \tag{112}$$

Lastly, the saturation regime results for the spherical wave are used,

$$\sigma_I^2 = 1 + \frac{2.73}{\sigma_1^{4/5}} = 1 + 2.92\left(\frac{k\rho_0^2}{L}\right)^{1/3} \,, \tag{113}$$

and is set equal to the *effective* scintillation index in the saturation regime limit [1],

$$\sigma_I^2 = \exp\left[\sigma_{\ln x}^2 + \sigma_{\ln y}^2\right] - 1 \approx \exp\left[2\sigma_{\ln x}^2\right] - 1 \approx 1 + \frac{1.76}{\sigma_1^{4/5}}\left(\frac{1}{c_2}\right)^{7/6} \,. \tag{114}$$

Therefore, $c_2 = .02$. Using these constants in the non-dimensional cutoffs, the following results are presented,

$$\eta_x = \frac{1}{9 + .02L/k\rho_0^2} = \frac{8.56}{1 + .19\sigma_1^{12/5}} \tag{115}$$

$$\eta_y = 9 + 1.7\frac{L}{k\rho_0^2} = 9\left(1 + .23\sigma_1^{12/5}\right). \tag{116}$$

Placing these cutoffs into (107) and (108) yields a scintillation index valid from weak-to-strong turbulence for a spherical wave along a horizontal propagation path,

$$\sigma_I^2\left(L\right)=\exp\left[\sigma_{\ln x}^2+\sigma_{\ln y}^2\right]-1$$
$$=\exp\left[\frac{0.2\sigma_1^2}{\left(1+.19\sigma_1^{12/5}\right)^{7/6}}+\frac{0.2\sigma_1^2}{\left(1+0.23\sigma_1^{12/5}\right)^{5/6}}\right]-1,\quad 0\le\sigma_1^2<\infty. \quad (117)$$

If we replace the Rytov variance with the weak scintillation index for the spherical wave, $\beta_0 = 0.4\sigma_I^2$, (117) becomes

$$\sigma_I^2\left(L\right)=\exp\left[\sigma_{\ln x}^2+\sigma_{\ln y}^2\right]-1$$
$$=\exp\left[\frac{0.49\beta_0^2}{\left(1+0.56\beta_0^{12/5}\right)^{7/6}}+\frac{0.51\beta_0^2}{\left(1+0.69\beta_0^{12/5}\right)^{5/6}}\right]-1, \quad (118)$$

which more closely resembles the coefficients present in the plane wave case. This result was originally derived by Andrews et. al. [2]. Figure 5 presents a comparison between the weak and *effective* scintillation indices. It should come to no surprise that the behavior is markedly similar to the plane wave case. The noticeable difference by comparing Figure 5 with Figure 3 is that the *effective* scintillation for the spherical wave has a higher maxima value.

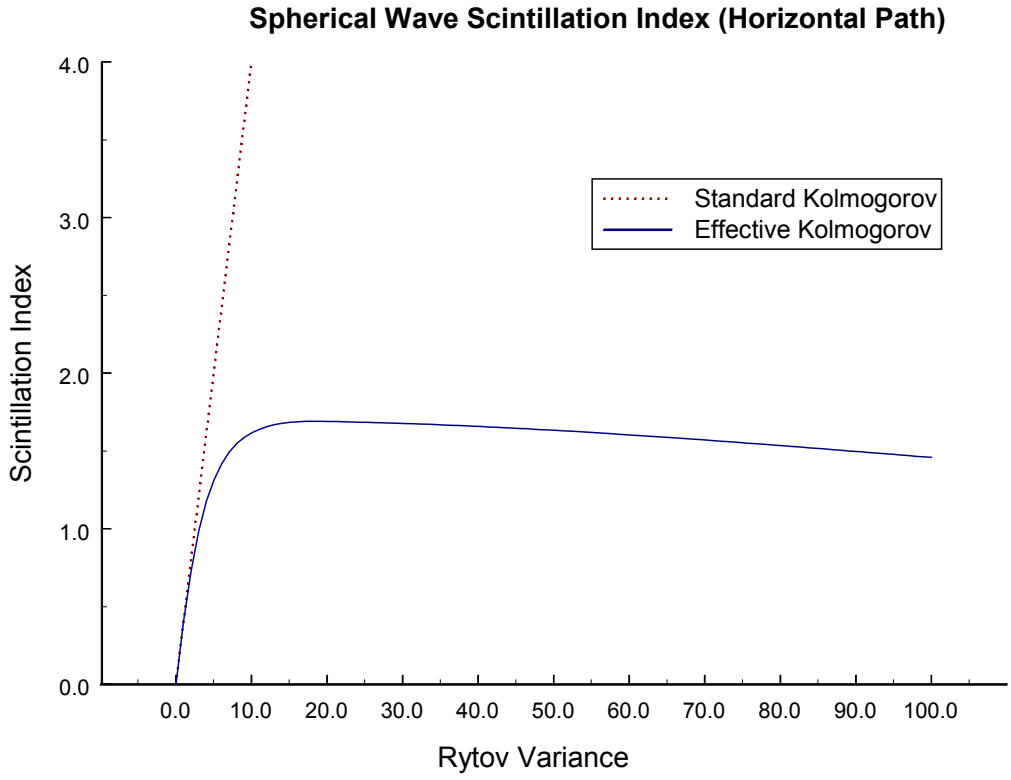

Figure 5: Comparison graph of weak (102) versus *effective* (118) plane wave results, based on Rytov Variance, σ_1^2.

6.3 Standard Kolmogorov, Slant Path

Unlike the plane wave case, where it is used for downlink scenarios, spherical waves are used for uplink scenarios. As mentioned at the beginning of this section, the spherical wave model lends itself to cases where the atmospheric turbulence is near the beginning of the propagation path. Propagating long distances magnifies the changes in the optical beam induced by atmospheric turbulence near the receiver. As in the plane wave case, the von Karman spectrum is used to bypass the discontinuities faced with the Kolmogorov spectrum. Also, the normalized distance

in uplink scenarios is defined by $\xi = 1 - (h - h_0)/(H - h_0)$. The slant path definition of the scintillation index is given as

$$\sigma_I^2 = 8\pi^2 k^2 \sec(\zeta) \int_{h_0}^{H} \int_{0}^{\infty} \kappa \Phi_n(h,\kappa) \left[1 - \cos\left(\frac{L\kappa^2}{k} \xi(1-\xi) \right) \right] d\kappa dh \quad . \quad (119)$$

Inserting the von Karman spectrum (6) with H-V C_n^2 (32) yields

$$\sigma_I^2 = 2.606 k^2 \sec(\zeta) \int_{h_0}^{H} C_n^2(h) \int_{0}^{\infty} \kappa \frac{\exp\left[-\kappa^2 / \kappa_m^2 \right]}{\left(\kappa^2 + \kappa_0^2 \right)^{11/6}} \times \left[1 - \cos\left(\frac{L\kappa^2}{k} \xi(1-\xi) \right) \right] d\kappa dh \quad . \quad (120)$$

Yet again, a previously derived result is employed on (120) to find

$$\sigma_I^2 = 1.303 k^2 \kappa_0^{-5/3} \sec(\zeta) \int_{h_0}^{H} C_n^2(h) \times \mathrm{Re}\left[U\left(1; \frac{1}{6}; \frac{\kappa_0^2}{\kappa_m^2} \right) - U\left(1; \frac{1}{6}; \kappa_0^2 \left(\frac{1}{\kappa_m^2} + \frac{iL}{k} \xi(1-\xi) \right) \right) \right] dh \quad . \quad (121)$$

By making a small argument approximation on each confluent hypergeometric function, the scintillation index can be simplified to

$$\sigma_I^2 = 1.303 k^2 \sec(\zeta) \int_{h_0}^{H} C_n^2(h) \Gamma(-1/6) \times \mathrm{Re}\left[\left(\frac{1}{\kappa_m^2} \right)^{5/6} - \left(\left(\frac{1}{\kappa_m^2} + \frac{iL}{k} \xi(1-\xi) \right) \right)^{5/6} \right] dh \quad . \quad (122)$$

By letting the outer scale cutoff go to infinity, the $1/\kappa_m^2$ terms drop out and leave behind

$$\sigma_I^2 = 8.825\,\mathrm{Re}\left(i^{5/6}\right)k^{7/6}L^{5/6}\sec(\zeta)\int_{h_0}^{H} C_n^2(h)\xi^{5/6}\left(1-\xi\right)^{5/6}dh\,. \tag{123}$$

Given that $L = (H - h_0)$ sec ζ, the uplink scintillation index originally derived by Andrews and Philips is given by [1]

$$\sigma_I^2 = 2.25k^{7/6}\mu_3\left(H-h_0\right)^{5/6}\sec^{11/6}\left(\zeta\right), \tag{124}$$

where μ_3 is defined as

$$\mu_3 = \int_{h_0}^{H} C_n^2(h)\xi^{5/6}\left(1-\xi\right)^{5/6}dh\,. \tag{125}$$

Due to a similar functional form as μ_1 (79), μ_3 can be closely approximated by it for calculations.

6.4 *Effective* Kolmogorov, Slant Path

For the *effective* spectrum along a slant path, a similar method is undertaken as in the plane wave case. First, separate the scintillation index into its large-scale and small-scale components respectively, again using the filter function and C_n^2model described in section 4.2

$$\begin{aligned}\sigma_{\ln y}^2 = {} & 2.606B\left(H,h_0\right)k^2\sec(\zeta)\int_{h_0}^{H} C_n^2\left(h\right)\int_0^{\infty}\frac{\kappa}{\left(\kappa^2+\kappa_y^2\right)^{11/6}} \\ & \times\left\{1-\cos\left[\frac{L\kappa^2}{k}\xi\left(1-\xi\right)\right]\right\}d\kappa dh\end{aligned} \tag{126}$$

$$\sigma_{\ln x}^2 = 2.606k^2 \sec(\zeta) \int_{h_0}^{H} C_n^2(h) \int_0^{\infty} \kappa^{-8/3} G_x(\kappa, z; H, h_0) \times \left\{1 - \cos\left[\frac{L\kappa^2}{k}\xi(1-\xi)\right]\right\} d\kappa dh \quad . \tag{127}$$

Consider the small-wave component first. Due to the small argument approximation used, (126) becomes equivalent to its plane wave counterpart (80), yielding

$$\begin{aligned}\sigma_{\ln y}^2 &= 1.56B(H, h_0)\mu_0 k^{7/6}(H - h_0)^{5/6} \sec^{11/6}(\zeta)\eta_y^{-5/6} \\ &= 0.7B(H, h_0)\left(\frac{\mu_0}{\mu_3}\right)\sigma_2^2 \eta_y^{-5/6}\end{aligned} \quad , \tag{128}$$

where σ_2^2 is the weak slant path scintillation index for a spherical wave (124). By setting (128) equal to the horizontal effective result, solving for B results in

$$B(H, h_0) = 4.54\frac{\mu_3}{\mu_0} \, . \tag{129}$$

For the large-wave portion, the spatial filter function, G_x must be calculated,

$$\begin{aligned}G_x(\kappa, z) &= A(H, h_0)\exp\left\{-2\left(\frac{\kappa}{\kappa_x}\right)^{5/3}\left[\left(1-\frac{z}{L}\right)^{5/3}\int_0^{z/L}\tau^{5/3}d\tau + \left(\frac{z}{L}\right)^{5/3}\int_{z/L}^{1}(1-\tau)^{5/3}d\tau\right]\right\} \\ &= A(H, h_0)\exp\left\{-\frac{3}{4}\left(\frac{\kappa}{\kappa_x}\right)^{5/3}\left[\left(1-\frac{z}{L}\right)^{5/3}\left(\frac{z}{L}\right)^{8/3} + \left(\frac{z}{L}\right)^{5/3}\left(1-\frac{z}{L}\right)^{8/3}\right]\right\} \\ &= A(H, h_0)\exp\left\{-\frac{3}{4}\left(\frac{\kappa}{\kappa_x}\right)^{5/3}\left(\frac{z}{L}\right)^{5/3}\left(1-\frac{z}{L}\right)^{5/3}\right\}\end{aligned} \quad . \tag{130}$$

Incorporating the filter function and a geometric optics approximation, the large-scale component becomes

$$\sigma_{\ln x}^2 = 1.3A\left(H,h_0\right)\left(H-h_0\right)^2 \sec^3\left(\zeta\right)\int_{h_0}^{H} C_n^2\left(h\right)\left(\frac{z}{L}\right)^2\left(1-\frac{z}{L}\right)^2$$
$$\times\int_0^{\infty}\kappa^{4/3}\exp\left\{-\frac{3}{4}\left(\frac{\kappa}{\kappa_x}\right)^{5/3}\left(\frac{z}{L}\right)^{5/3}\left(1-\frac{z}{L}\right)^{5/3}\right\}d\kappa dh \quad . \qquad (131)$$

Using a change of variable along with the integral definition of the gamma function, (148) simplifies to

$$\sigma_{\ln x}^2 = .78A\left(H,h_0\right)\left(H-h_0\right)^2 \sec^3\left(\zeta\right)3\Gamma\left(\frac{7}{5}\right)$$
$$\times\int_{h_0}^{H} C_n^2\left(h\right)\left(\frac{z}{L}\right)^2\left(1-\frac{z}{L}\right)^2\left\{\frac{3}{4}\kappa_x^{-5/3}\left(\frac{z}{L}\right)^{5/3}\left(1-\frac{z}{L}\right)^{5/3}\right\}^{-7/5} dh \quad . \qquad (132)$$

Introduce a new parameter, μ_4, which is defined as

$$\mu_4 = \int_{h_0}^{H} C_n^2\left(h\right)\left(\frac{z}{L}\right)^{-1/3}\left(1-\frac{z}{L}\right)^{-1/3} dh \quad . \qquad (133)$$

Using this new parameter and further algebraic simplification, the large-scale component becomes

$$\sigma_{\ln x}^2 = 1.04A\left(H,h_0\right)\left(H-h_0\right)^{5/6} k^{7/6}\eta_x^{\ 7/6}\sec^{11/6}\left(\zeta\right)\mu_4$$
$$= 0.46A\left(H,h_0\right)\left(\frac{\mu_4}{\mu_3}\right)\sigma_2^2\eta_x^{\ 7/6} \quad . \qquad (134)$$

Setting (134) equivalent to its horizontal counterpart yields

$$A\left(H,h_0\right)=9.31\frac{\mu_3}{\mu_4}. \tag{135}$$

Recalling the non-dimensional cutoffs derived in the *effective* horizontal section, inserting those along with the weighting constants gives the *effective* scintillation index for a spherical wave along a slant path,

$$\begin{aligned}\sigma_I^2\left(L\right)&=\exp\left[\sigma_{\ln x}^2+\sigma_{\ln y}^2\right]-1\\&=\exp\left[\frac{0.49\sigma_2^2}{\left(1+0.56\sigma_2^{12/5}\right)^{7/6}}+\frac{0.51\sigma_2^2}{\left(1+0.69\sigma_2^{12/5}\right)^{5/6}}\right]-1,\quad 0\le\sigma_2^2<\infty,\end{aligned} \tag{136}$$

which was first derived by Andrews et. al. [2]. One notices how similar this result is to the horizontal case down to the coefficients. Although this *effective* uplink scintillation index has different results than its downlink counterpart, they both yield the same results in the weak fluctuation regime. Figure 6 compares both slant path cases. As expected, the general behavior parallels the downlink case.

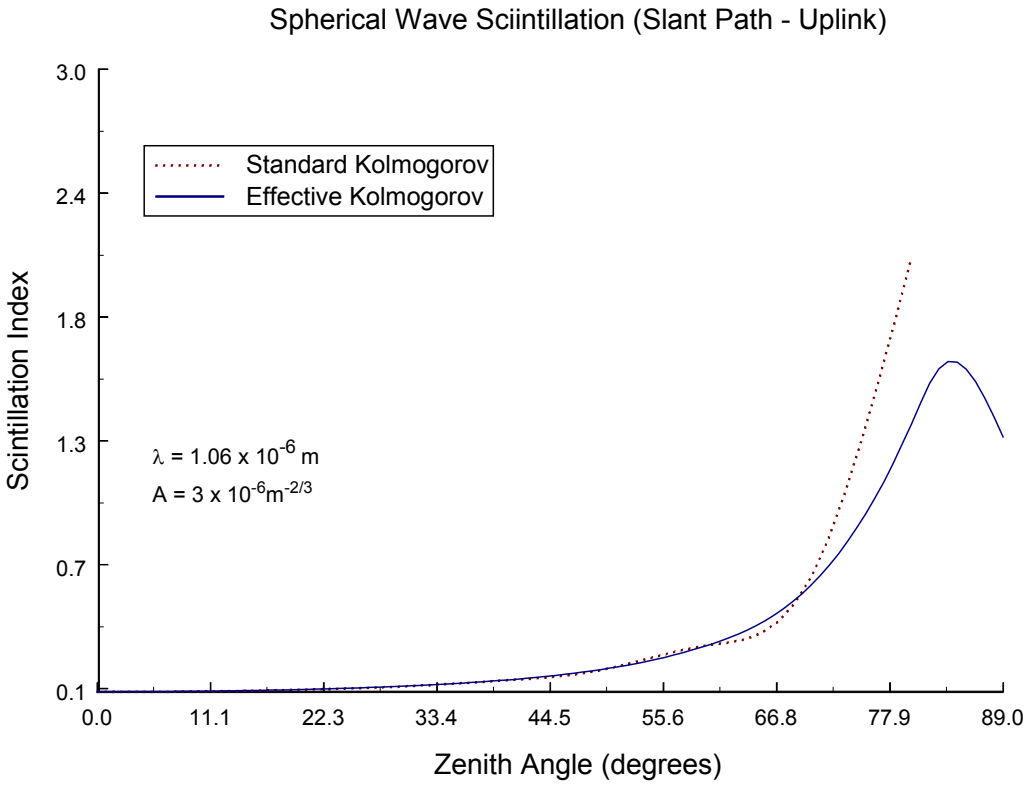

Figure 6: Comparison of weak (124) versus *effective* (136) spherical wave scintillation for uplink path.

CHAPTER 7: SCINTILLATION INDEX - GAUSSIAN BEAM WAVE

The previous sections dealt with the plane wave and spherical wave models. Each of these gives a rough idea of how an optical beam will react to turbulence, but are not realistic; one is infinitely long, while the other is an infinitesimal point source. The Gaussian beam wave case is the most realistic of the three, but also the most complex to use for calculations. Recall the scintillation index (43) presented earlier

$$\sigma_I^2(\mathbf{r},L) = 8\pi^2 k^2 L \int_0^1 \int_0^\infty \kappa \Phi_n(\kappa) e^{-\frac{\Lambda L \kappa^2 \xi^2}{k}} \times \left\{ I_0(2\Lambda r \kappa \xi) - \cos\left[\frac{L\kappa^2}{k} \xi \left(1 - \bar{\Theta}\xi\right) \right] \right\} d\kappa d\xi ,$$

where r is the beam radius. This is usually separated into two different integrals,

$$\sigma_{I,r}^2(\mathbf{r},L) = 8\pi^2 k^2 L \int_0^1 \int_0^\infty \kappa \Phi_n(\kappa) e^{-\frac{\Lambda L \kappa^2 \xi^2}{k}} \left\{ I_0(2\Lambda r \kappa \xi) - 1 \right\} d\kappa d\xi \qquad (137)$$

$$\sigma_{I,l}^2(\mathbf{r},L) = 8\pi^2 k^2 L \int_0^1 \int_0^\infty \kappa \Phi_n(\kappa) e^{-\frac{\Lambda L \kappa^2 \xi^2}{k}} \left\{ 1 - \cos\left[\frac{L\kappa^2}{k} \xi \left(1 - \bar{\Theta}\xi\right) \right] \right\} d\kappa d\xi , \qquad (138)$$

the radial (off-axis) and longitudinal (on-axis) components respectively. The reasoning is twofold. This allows a more direct comparison to the spherical and plane wave cases, which by the nature of the models themselves, on-axis only. Secondly, this separation is more manageable for calculations than the form presented in (43). These equations will be used for the following four cases [1].

7.1 Standard Kolmogorov, Horizontal Path

Like the plane and spherical wave cases, the von Karman spectrum (6) is used for the on-axis portion of the scintillation index to find the Kolmogorov results. However, the Kolmogorov spectrum (4) is used directly in the radial component. This is due to the exponential term present in the Gaussian beam wave case that prevents the discontinuities from occurring. Inserting each spectrum into their proper component yields

$$\sigma_{I,r}^2\left(\mathbf{r},L\right)=0.6514C_n^2k^2L\int_0^1\int_0^\infty \kappa^{-8/3}\exp\left(-\frac{\Lambda L\kappa^2\xi^2}{k}\right)\left\{I_0\left(2\Lambda r\kappa\xi\right)-1\right\}d\kappa d\xi \quad (139)$$

$$\sigma_{I,l}^2\left(\mathbf{r},L\right)=2.6056C_n^2k^2L\int_0^1\int_0^\infty \kappa\frac{\exp\left[-\kappa^2/\kappa_m^2\right]}{\left(\kappa^2+\kappa_0^2\right)^{11/6}}\exp\left(-\frac{\Lambda L\kappa^2\xi^2}{k}\right)\times\left\{1-\cos\left[\frac{L\kappa^2}{k}\xi\left(1-\bar{\Theta}\xi\right)\right]\right\}d\kappa d\xi \quad (140)$$

Start with the radial component, and replace the modified Bessel function with its series representation,

$$\sigma_{I,r}^2\left(\mathbf{r},L\right)=0.6514C_n^2k^2L\sum_{k=1}^{\infty}\frac{\left(\Lambda r\right)^{2k}}{k!\Gamma\left(k+1\right)}\int_0^1\int_0^\infty \kappa^{2k-8/3}\xi^{2k}\exp\left(-\frac{\Lambda L\kappa^2\xi^2}{k}\right)d\kappa d\xi \quad (141)$$

Noticing that the kappa integration is in the form of a gamma function,

$$\sigma_{I,r}^2\left(\mathbf{r},L\right)=0.3257C_n^2k^2L\sum_{k=1}^{\infty}\frac{\left(\Lambda r\right)^{2k}}{k!\Gamma\left(k+1\right)}\int_0^1\xi^{2k}\frac{\Gamma\left(k-5/6\right)}{\left(\frac{\Lambda L\xi^2}{k}\right)^{k-5/6}}d\xi \quad (142)$$

Performing the rudimentary integration yields,

$$\sigma_r^2\left(\mathbf{r},L\right)=0.1777C_n^2k^{7/6}L^{11/6}\Lambda^{5/6}\sum_{k=1}^{\infty}\left(\frac{\Lambda r^2k}{L}\right)^k\frac{\Gamma\left(k-5/6\right)}{k!\Gamma\left(k+1\right)} \tag{143}$$

Making a substitution for spot size, W, and Rytov variance simplifies the radial component to

$$\sigma_r^2\left(\mathbf{r},L\right)=0.1445\sigma_1^2\Lambda^{5/6}\sum_{k=1}^{\infty}\left(\frac{2r^2}{W^2}\right)^k\frac{\Gamma\left(k-5/6\right)}{k!\Gamma\left(k+1\right)}. \tag{144}$$

Here, we introduce the Pochammer symbol, which is closely tied to the gamma function [1],

$$\left(a\right)_n=\frac{\Gamma\left(a+n\right)}{\Gamma\left(n\right)},\quad n=1,2,3,4,\ldots. \tag{145}$$

By substituting the gamma function for Pochammer symbol and shifting the series from $k = 1$ to $k = 0$, we arrive at

$$\sigma_{I,r}^2\left(\mathbf{r},L\right)=0.663\sigma_1^2\Lambda^{5/6}\left[1-\sum_{k=0}^{\infty}\left(\frac{2r^2}{W^2}\right)^k\frac{\left(-5/6\right)_k}{\left(1\right)_k\,k!}\right], \tag{146}$$

where the series is in the precise form of a hypergeometric function. Therefore the radial component of the scintillation index in weak fluctuations is

$$\begin{aligned}\sigma_{I,r}^2\left(\mathbf{r},L\right)&=2.65\sigma_1^2\Lambda^{5/6}\left[1-{}_1F_1\left(-\frac{5}{6};1;\frac{2r^2}{W^2}\right)\right]\\&\approx 4.42\sigma_1^2\Lambda^{5/6}\frac{r^2}{W^2}\end{aligned}. \tag{147}$$

For the longitudinal case, separate it into two integrals,

$$\sigma_{I,l}^2\left(\mathbf{r},L\right)=2.6056C_n^2k^2L\left[I_1-I_2\right]$$

$$I_1=\int_0^1\int_0^\infty \kappa\frac{d\kappa d\xi}{\left(\kappa^2+\kappa_0^2\right)^{11/6}}\exp\left(-\kappa^2\left[\frac{1}{\kappa_m^2}+\frac{\Lambda L\xi^2}{k}\right]\right) \quad . \qquad (148)$$

$$I_2=\int_0^1\int_0^\infty \kappa\frac{\exp\left[-\kappa^2\left(\frac{1}{\kappa_m^2}+\frac{\Lambda L\xi^2}{k}\right)\right]}{\left(\kappa^2+\kappa_0^2\right)^{11/6}}\cos\left[\frac{L\kappa^2}{k}\xi\left(1-\bar{\Theta}\xi\right)\right]d\kappa d\xi$$

Start with I_1 and employ the same known integral relation and small argument approximation as the other weak horizontal cases. This results in

$$I_1=\frac{\kappa_0^{-5/3}}{2}\left(\frac{6}{5}+\Gamma\left(-5/6\right)\kappa_0^{5/3}\int_0^1\left[\left(\frac{1}{\kappa_m^2}+\frac{\Lambda L\xi^2}{k}\right)\right]^{5/6}d\xi\right) \qquad (149)$$

By letting the outer scale go to infinity and performing the integration,

$$I_1=\frac{3}{5}\kappa_0^{-5/3}-5\left(\frac{\Lambda L}{k}\right)^{5/6} \quad . \qquad (150)$$

Return to I_2. Replace the cosine term with a complex exponential,

$$I_2=\mathrm{Re}\left[\int_0^1\int_0^\infty \kappa\frac{\exp\left[-\kappa^2\left(\frac{1}{\kappa_m^2}+\frac{\Lambda L\xi^2}{k}+\frac{iL}{k}\xi\left(1-\bar{\Theta}\xi\right)\right)\right]}{\left(\kappa^2+\kappa_0^2\right)^{11/6}}d\kappa d\xi\right], \qquad (151)$$

and perform the same procedure as in the I_1 case,

$$I_2 = \mathrm{Re}\left[\frac{\kappa_0^{-5/3}}{2}\left(\frac{6}{5}+\Gamma\left(-5/6\right)\kappa_0^{5/3}\int_0^1\left[\left(\frac{1}{\kappa_m^2}+\frac{\Lambda L\xi^2}{k}+\frac{iL}{k}\xi\left(1-\bar{\Theta}\xi\right)\right)\right]^{5/6}d\xi\right)\right]. \quad (152)$$

Let the outer scale go to infinity,

$$I_2 = \frac{3}{5}\kappa_0^{-5/3}+\mathrm{Re}\left[\left(\Gamma\left(-5/6\right)\left(\frac{L}{k}\right)^{5/6}\int_0^1\xi^{5/6}\left[\left(\Lambda-i\bar{\Theta}\right)\xi+i\right]^{5/6}d\xi\right)\right]. \quad (153)$$

Here, we introduce another integral relation [1],

$$\int_0^x\frac{t^{u-1}}{\left(1+\beta t\right)^v}dt=\frac{x^u}{u}\,{}_2F_1\left(v,u;1+u;-\beta x\right),u>0\,. \quad (154)$$

By using this relation, I_2 reduces to

$$I_2 = \frac{3}{5}\kappa_0^{-5/3}+1.48\,\mathrm{Re}\left[i^{5/6}\,{}_2F_1\left(-\frac{5}{6},\frac{11}{6};\frac{17}{6};\bar{\Theta}+i\Lambda\right)\right] \quad (155)$$

Combining I_1 and I_2 results in the longitudinal component,

$$\sigma_{I,l}^2 = 3.86\sigma_1^2\,\mathrm{Re}\left[i^{5/6}\,{}_2F_1\left(-\frac{5}{6},\frac{11}{6};\frac{17}{6};\bar{\Theta}+i\Lambda\right)\right]-0.688\Lambda^{5/6}\,. \quad (156)$$

Note that by setting theta and lambda to their spherical or plane wave values, one can go back to the results already derived. A full expression for the scintillation index is given by combining the radial and longitudinal components,

$$\begin{aligned}\sigma_I^2 &= 4.42\sigma_1^2\Lambda^{5/6}\frac{r^2}{W^2}+\\ &\quad 3.86\sigma_1^2\,\mathrm{Re}\left[i^{5/6}\,{}_2F_1\left(-\frac{5}{6},\frac{11}{6};\frac{17}{6};\bar{\Theta}+i\Lambda\right)\right]-0.688\Lambda^{5/6},\end{aligned} \quad (157)$$

which is equivalent to the result found by Andrews and Phillips [1].

7.2 *Effective* Kolmogorov, Horizontal Path

While the approach to the longitudinal portion of the scintillation index will mirror the plane and spherical wave cases, the radial component is dependent on the work of Miller et. al. [1]. Their work details a tractable method of extending standard Kolmogorov results into the moderate-to-strong regimes of turbulence. *Effective* beam parameters were formulated to account for the additional broadening of the beam due to stronger turbulence. These new parameters are defined as

$$W_e = W\left(1+1.63\sigma_1^{12/5}\Lambda\right)^{1/2} \tag{158}$$

$$F_e = -\frac{L\left(1+1.63\sigma_1^{12/5}\Lambda\right)}{\bar{\Theta}+2.44\sigma_1^{12/5}\Lambda} \tag{159}$$

$$\Lambda_e = \frac{2L}{kW_e^2} = \frac{\Lambda}{1+1.63\sigma_1^{12/5}\Lambda} \tag{160}$$

$$\Theta_e = 1+\frac{L}{F_e} = \frac{\Theta-.81\sigma_1^{12/5}\Lambda}{1+1.63\sigma_1^{12/5}\Lambda}, \quad \bar{\Theta}_e = 1-\Theta_e. \tag{161}$$

Note that these *effective* parameters reduce to Λ and Θ under weak fluctuations. By replacing beam parameter Λ into the radial scintillation index for weak fluctuations,

$$\sigma_{I,r}^2\left(\mathbf{r},L\right)=2.65\sigma_1^2\Lambda_e^{5/6}\left[1-{}_1F_1\left(-\frac{5}{6};1;\frac{2r^2}{W_e^2}\right)\right]$$
$$\approx 4.42\sigma_1^2\Lambda_e^{5/6}\frac{r^2}{W_e^2} \tag{162}$$

Now, consider the longitudinal component. As per the plane and spherical wave cases, after inserting the *effective* Kolmogorov spectrum (28), the index is split up into large-scale and small-scale components. However, a slight modification has been made to the small-scale filter function as noted,

$$G_y\left(\kappa\right)=\frac{\kappa^{11/3}\exp\left[\Lambda\kappa^2\xi^2/L\right]}{\left(\kappa^2+\kappa_y^2\right)^{11/6}} \tag{163}$$

where $\xi = 1 - z/L$. Therefore,

$$\sigma_{\ln y}^2\left(\mathbf{r},L\right)=2.6056C_n^2k^2L\int_0^1\int_0^\infty\frac{\exp\left[\frac{\Lambda L\kappa^2\xi^2}{k}\right]}{\left(\kappa^2+\kappa_y^2\right)^{11/6}}\exp\left[-\frac{\Lambda L\kappa^2\xi^2}{k}\right]$$
$$\times\left\{1-\cos\left[\frac{L\kappa^2}{k}\xi\left(1-\bar{\Theta}\xi\right)\right]\right\}d\kappa d\xi \tag{164}$$
$$=2.6056C_n^2k^2L\int_0^1\int_0^\infty\left(\kappa^2+\kappa_y^2\right)^{-11/6}\left\{1-\cos\left[\frac{L\kappa^2}{k}\xi\left(1-\bar{\Theta}\xi\right)\right]\right\}d\kappa d\xi$$

$$\sigma_{\ln x}^2\left(\mathbf{r},L\right)=2.6056C_n^2k^2L\int_0^1\int_0^\infty\kappa^{-11/3}\exp\left[-\frac{\kappa^2}{\kappa_x^2}\right]\exp\left[-\frac{\Lambda\kappa^2\xi^2}{k}\right]$$
$$\times\left\{1-\cos\left[\frac{L\kappa^2}{k}\xi\left(1-\bar{\Theta}\xi\right)\right]\right\}d\kappa d\xi \tag{165}$$

Apply a geometrical optics approximation in the large-scale case, which leaves the first two terms of the series expansion of the 1- cosine term. For the small-scale scintillation, the heavily damped oscillation results in the cosine term being negligible. In addition, the lambda-dependent exponential term in the large-scale index dies out quickly, so it can be neglected. The indices are reduced to

$$\sigma_{\ln y}^2 \approx 2.6056 C_n^2 k^2 L \int_0^1 \int_0^\infty \frac{d\kappa d\xi}{\left(\kappa^2 + \kappa_y^2\right)^{11/6}} \tag{166}$$

$$\begin{aligned} \sigma_{\ln x}^2 &\approx 2.6056 C_n^2 k^2 L \int_0^1 \int_0^\infty \kappa^{-11/3} \exp\left[-\frac{\kappa^2}{\kappa_x^2}\right]\left[\frac{L\kappa^2}{k}\xi\left(1-\bar{\Theta}\xi\right)\right]^2 d\kappa d\xi \\ &= 2.6056 C_n^2 L^3 \int_0^1 \xi^2 \left(1-\bar{\Theta}\xi\right)^2 d\xi \int_0^\infty \kappa^{1/3} \exp\left[-\frac{\kappa^2}{\kappa_x^2}\right] d\kappa \end{aligned}, \tag{167}$$

where the small-scale component is now equivalent to its spherical wave counterpart. Therefore, we can rewrite (166) as

$$\sigma_{\ln y}^2 = 1.27 \sigma_1^2 \eta_y^{-5/6}. \tag{168}$$

Performing the integrations in the large-scale component, noting the kappa integration is in the form of a gamma function, yields

$$\begin{aligned} \sigma_{\ln x}^2 &= \frac{2.6056}{2}\Gamma\left(\frac{7}{6}\right) C_n^2 L^3 \kappa_x^{7/3}\left(\frac{1}{3}-\frac{1}{2}\bar{\Theta}+\frac{1}{5}\bar{\Theta}^2\right) \\ &= .49\left(\frac{1}{3}-\frac{1}{2}\bar{\Theta}+\frac{1}{5}\bar{\Theta}^2\right)\sigma_1^2 \eta_x^{7/6} \end{aligned}. \tag{169}$$

For calculating the non-dimensional cutoffs, a similar approach is used as laid out in the plane wave and spherical wave cases. For η_y, the small-scale index is set equal to the weak scintillation index, and ln 2 for the saturation regime. This results in

$$\eta_y = 3\left[\left(\frac{\sigma_1}{\sigma_B}\right)^{12/5} + 0.69\sigma_2^{12/5}\right]. \tag{170}$$

Similarly for the large-scale case,

$$\begin{aligned}\eta_x &= \left(\frac{1}{3}-\frac{1}{2}\bar{\Theta}+\frac{1}{5}\bar{\Theta}^2\right)\left(\frac{\sigma_1^2}{\sigma_B^2}\right)^{12/7} + 1.12\left(\frac{\frac{1}{3}-\frac{1}{2}\bar{\Theta}+\frac{1}{5}\bar{\Theta}^2}{1+2.18\bar{\Theta}}\right)^{6/7}\sigma_1^{12/5}, \\ &\approx \left(\frac{1}{3}-\frac{1}{2}\bar{\Theta}+\frac{1}{5}\bar{\Theta}^2\right)\left(\frac{\sigma_1^2}{\sigma_B^2}\right)^{12/7}\left(1+.56\sigma_B^{12/5}\right)\end{aligned} \tag{171}$$

where σ_B^2 is the weak longitudinal scintillation for a Gaussian beam and the term, $1.12(\sigma_l/\sigma_B)^{24/35}/(1+2.18(1-\Theta))^{6/7}$,is approximated as .56, which is only exact in the limiting case of Θ = 0. Inserting these cutoffs and combining the small-scale and large-scale terms yields

$$\begin{aligned}\sigma_I^2(L) &= \exp\left[\sigma_{\ln x}^2 + \sigma_{\ln y}^2\right] - 1 \\ &= \exp\left[\frac{0.49\sigma_B^2}{\left(1+.56\sigma_B^{12/5}\right)^{7/6}} + \frac{0.51\sigma_B^2}{\left(1+0.69\sigma_B^{12/5}\right)^{5/6}}\right] - 1.\end{aligned} \tag{172}$$

Combining the longitudinal and radial components leads to

$$\sigma_I^2\left(L\right)=4.42\sigma_1^2\Lambda_e^{5/6}\frac{r^2}{W_e^2}+$$
$$\exp\left[\frac{0.49\sigma_B^2}{\left(1+.56\sigma_B^{12/5}\right)^{7/6}}+\frac{0.51\sigma_B^2}{\left(1+0.69\sigma_B^{12/5}\right)^{5/6}}\right]-1, \tag{173}$$

an identical result as found by Andrews et. al. [2]. A comparison between the standard and *effective* scintillation indices is presented in Figure 7 for a collimated beam (Θ = 1) with varying propagation length. When comparing only the longitudinal portions, we note similar behavior exhibited in the plane and spherical wave cases. When adding the radial component, the separation between standard and *effective* results happens more quickly, as well as a hump appearing on the *effective* result after exiting the weak regime of turbulence. This is an unfortunate byproduct of the *effective* beam parameters, not providing a smooth transition from weak to moderate and strong results.

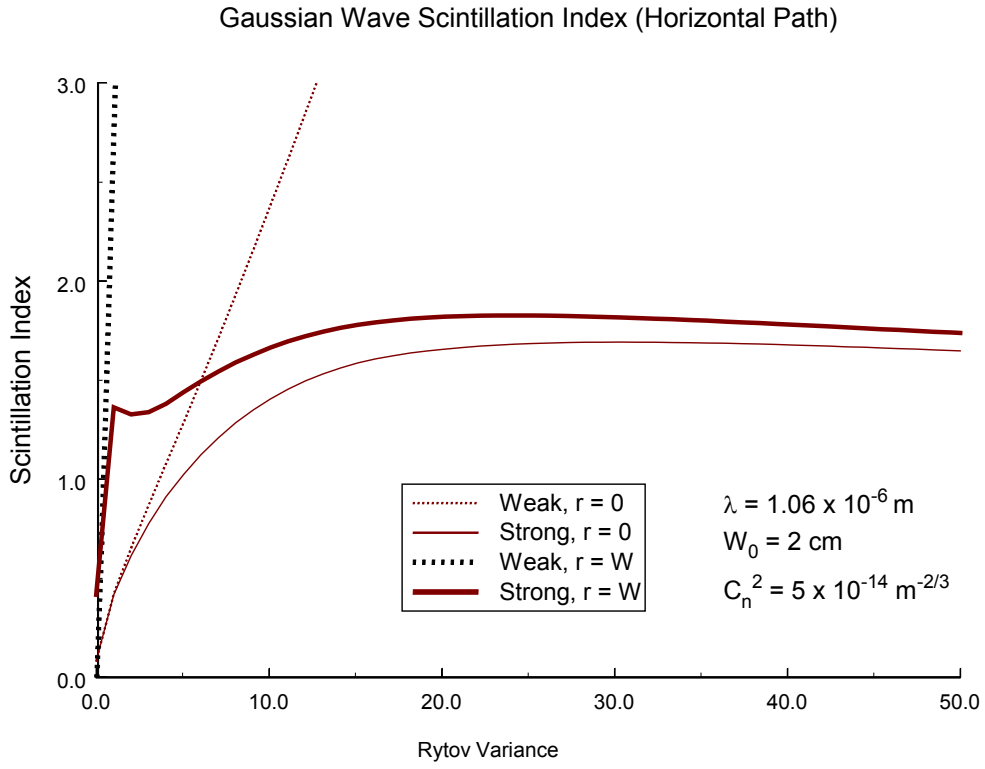

Figure 7: Comparison of weak (151) versus *effective* (173) Gaussian wave scintillation for horizontal path, varying σ_I^2.

7.3 Standard Kolmogorov, Slant Path

While the Gaussian beam wave model can be used to describe both uplink and downlink scenarios, the following derivation is performed for the uplink scenario. Therefore, the normalized distance parameter is $\xi = 1 - (h - h_0)/(H - h_0)$. (The downlink scenario's derivation is nearly equivalent.) Inserting the standard Kolmogorov spectrum (4) with the H-V model into the radial and longitudinal components yields

$$\sigma_{I,r}^2 = 2.606k^2 \sec(\zeta) \int_{h_0}^{H} C_n^2(h) \int_0^{\infty} \kappa^{-8/3} \exp\left(-\frac{\Lambda L \kappa^2 \xi^2}{k}\right) \times \left[I_0(2\kappa\Lambda\xi r) - 1\right] d\kappa dh \tag{174}$$

$$\sigma_{I,L}^2 = 2.606k^2 \sec(\zeta) \int_{h_0}^{H} C_n^2(h) \int_0^{\infty} \kappa^{-8/3} \exp\left(-\frac{\Lambda L \kappa^2 \xi^2}{k}\right) \times \left[1 - \cos\left[\frac{L\kappa^2}{k}\xi\left(1 - \bar{\Theta}\xi\right)\right]\right] d\kappa dh \,. \tag{175}$$

Start with the radial component. Replace the modified Bessel function with its series equivalent,

$$\sigma_{I,r}^2 = 2.606k^2 \sec(\zeta) \int_{h_0}^{H} C_n^2(h) \int_0^{\infty} \kappa^{-8/3} \exp\left(-\frac{\Lambda L \kappa^2 \xi^2}{k}\right) \times \sum_{n=1}^{\infty} \frac{(\kappa\Lambda\xi r)^{2n}}{(1)_n \, n!} d\kappa dh \,. \tag{176}$$

Note the kappa integral being in the form of a gamma function, and shift the series from $n = 1$ to $n = 0$,

$$\sigma_{I,r}^2 = 1.303k^2 \sec(\zeta)\left(\frac{\Lambda L}{k}\right)^{5/6} \Gamma(-5/6) \times \int_{h_0}^{H} \xi^{5/3} C_n^2(h)\left[\sum_{n=0}^{\infty} \frac{(-5/6)_n}{(1)_n\, n!}\left(\frac{k\Lambda r^2}{L}\right)^n - 1\right] dh. \quad (177)$$

Since (177) is in the form of a hypergeometric function, it can be rewritten as

$$\sigma_{I,r}^2 = -8.703k^{7/6}\Lambda^{5/6}L^{5/6}\sec(\zeta)\int_{h_0}^{H} C_n^2(h)\xi^{5/3}\left[{}_1F_1\left(-\frac{5}{6};1;-\frac{2r^2}{W^2}\right)-1\right]dh. \quad (178)$$

Using a small argument approximation, the hypergeometric function can be approximated,

$$\sigma_{I,r}^2 = -8.703k^{7/6}\Lambda^{5/6}L^{5/6}\sec(\zeta)\int_{h_0}^{H} C_n^2(h)\xi^{5/3}\frac{5r^2}{3W^2}dh, \quad (179)$$

where the altitude integral is in the form of μ_I from the spherical case. Therefore, the radial component simplifies to

$$\sigma_{I,r}^2 \approx 14.508\mu_1 k^{7/6}\Lambda^{5/6}(H-h_0)^{5/6}\sec^{11/6}(\zeta)\frac{r^2}{W^2}. \quad (180)$$

Return to the longitudinal portion, and replace the cosine term with its complex exponential definition and the 1 – exponential term with its series equivalent,

$$\sigma_{I,L}^2 = -2.606k^2 \sec(\zeta)\,\mathrm{Re}\left[\begin{array}{l}\int_{h_0}^{H} C_n^2(h)\sum_{n=1}^{\infty}\frac{1}{n!}\left[-\frac{iL}{k}\xi\left(1-\bar{\Theta}\xi\right)\right]^n \\ \times\int_0^{\infty}\kappa^{2n-8/3}\exp\left(-\frac{\Lambda L\kappa^2\xi^2}{k}\right)d\kappa dh\end{array}\right], \quad (181)$$

where the kappa integration is the same as in the radial derivation. Substituting this result along with shifting the series from $n = 1$ to $n = 0$ results in

$$\sigma_{I,L}^2 = 8.702k^{7/6}\Lambda^{5/6}L^{5/6}\sec(\zeta)\,\mathrm{Re}\left[\begin{array}{l}\int_{h_0}^{H}\xi^{5/3}C_n^2(h) \\ \times\left(\sum_{n=0}^{\infty}\frac{(-5/6)_n}{n!}\left[-i\frac{\left(1-\bar{\Theta}\xi\right)}{\Lambda\xi}\right]^n - 1\right)dh\end{array}\right]. \quad (182)$$

Noting that the series is equivalent to a binomial sum,

$$\sigma_{I,L}^2 = 8.702k^{7/6}L^{5/6}\sec(\zeta)\,\mathrm{Re}\left[\begin{array}{l}\int_{h_0}^{H}C_n^2(h) \\ \times\left(\xi^{5/6}\left[\Lambda\xi + i\left(1-\bar{\Theta}\xi\right)\right]^{5/6} - \Lambda^{5/6}\xi^{5/3}\right)dh\end{array}\right]. \quad (183)$$

Introduce new altitude integral, μ_3,

$$\mu_3 = \mathrm{Re}\left[\int_{h_0}^{H} C_n^2(h)\left(\xi^{5/6}\left[\Lambda\xi + i\left(1-\bar{\Theta}\xi\right)\right]^{5/6} - \Lambda^{5/6}\xi^{5/3}\right)dh\right]. \quad (184)$$

Therefore, the longitudinal component simplifies to

$$\sigma_{I,L}^2 = 8.702k^{7/6}\left(H-h_0\right)^{5/6}\sec^{11/6}(\zeta)\,\mu_3\,. \quad (185)$$

Combining the radial and longitudinal components leads to an equivalent result as found by Andrews and Phillips [1],

$$\sigma_I^2 = 8.702k^{7/6}\left(H-h_0\right)^{5/6}\sec^{11/6}\left(\zeta\right)\left[\mu_3 + 1.667\mu_1\Lambda^{5/6}\frac{r^2}{W^2}\right]. \qquad (186)$$

This form of the scintillation index makes apparent the similarity between the radial component of this case and the previous horizontal cases.

7.4 *Effective* Kolmogorov, Slant Path

Similar to the approach taken in the horizontal path case, the *effective* beam parameters are used to extend the radial scintillation index derived using the standard Kolmogorov spectrum to all regimes of turbulence. Inserting them into the standard radial expression, replacing the Rytov variance with the weak scintillation index for a Gaussian beam wave yields

$$\sigma_{I,r}^2 = 14.508\mu_1 k^{7/6}\Lambda_e^{5/6}\left(H-h_0\right)^{5/6}\sec^{11/6}\left(\zeta\right)\frac{r^2}{W_e^2}. \qquad (187)$$

Now, use the *effective* Kolmogorov spectrum in the scintillation index as described in section 4.2, separating it into large-scale and small-scale components

$$\begin{aligned}\sigma_{\ln I,y}^2\left(0,L\right) &= 8\times.033\pi^2k^2\sec\left(\zeta\right)\int_{h_0}^{H}\int_0^{\infty}C_n^2\left(h\right)\kappa\frac{B\left(H,h_0\right)\kappa^{11/3}}{\left(\kappa^2+\kappa_y^2\right)^{11/6}} \\ &\times\exp\left(\frac{\Lambda L\kappa^2\xi^2}{k}\right)\exp\left(-\frac{\Lambda L\kappa^2\xi^2}{k}\right)\left\{1-\cos\left[\frac{L\kappa^2}{k}\xi\left(1-\bar{\Theta}\xi\right)\right]\right\}d\kappa dh\end{aligned} \qquad (188)$$

$$\sigma^2_{\ln I,x}\left(\mathbf{r},L\right)=8\pi^2k^2\sec\left(\zeta\right)\int_{h_0}^{H}\int_{0}^{\infty}\exp\left(-\frac{\Lambda L\kappa^2\xi^2}{k}\right)\left\{1-\cos\left[\frac{L\kappa^2}{k}\xi\left(1-\bar{\Theta}\xi\right)\right]\right\}\times \\ A\left(H,h_0\right).033C_n^2\left(h\right)\kappa^{-8/3}G_x\left(\kappa,z;H,h_0\right)d\kappa dh \quad (189)$$

For the small-wave case, using the aforementioned damped oscillation approximation as well as canceling out the exponential terms, (188) reduces down to its spherical wave counterpart,

$$\sigma^2_{\ln y}=2.61k^2B\left(H,h_0\right)\sec\left(\zeta\right)\int_{h_0}^{H}C_n^2\left(h\right)\int_{0}^{\infty}\frac{\kappa}{\left(\kappa^2+\kappa_y^2\right)^{11/6}}d\kappa dh\cdot \quad (190)$$

With this knowledge, (188) reduces to

$$\sigma^2_{\ln y}\approx 1.56k^{7/6}\left(H-h_0\right)^{5/6}B\left(H,h_0\right)\eta_y^{-5/6}\sec^{11/6}\left(\zeta\right)\mu_0 \\ =0.695B\left(H,h_0\right)\eta_y^{-5/6}\frac{\mu_0}{\mu_3}\sigma_2^2 \quad , \quad (191)$$

where σ_2^2 is the weak scintillation for a spherical beam along a slant path. To find the weighting constant, B, we set this equivalent to horizontal beam results,

$$\sigma^2_{\ln y}=1.27\sigma_1^2\eta_y^{-5/6},$$

leading to

$$B=4.535\frac{\mu_1}{\mu_0}. \quad (192)$$

Return to the large-scale case. First, the spatial filter function, G_x, needs to be evaluated for the Gaussian beam wave case. Thus,

$$
\begin{aligned}
G_x &= A(H,h_0)\exp\left\{-\int_0^1 D\left[\frac{\kappa\rho_0}{\kappa_x}w(\tau,z)\right]d\tau\right\} \\
&= A(H,h_0)\exp\left\{-2\left(\frac{\kappa}{\kappa_x}\right)^{5/3}\left[\int_0^{z/L}\tau^{5/3}\left(1-\frac{\bar{\Theta}z}{L}\right)^{5/3}d\tau+\int_{z/L}^1\left(\frac{z}{L}\right)^{5/3}\left(1-\bar{\Theta}\tau\right)^{5/3}d\tau\right]\right\} \\
&= A(H,h_0)\exp\left\{\frac{3}{8}\left(\frac{z}{L}\right)^{8/3}\left(1-\frac{\bar{\Theta}z}{L}\right)^{5/3}-\frac{3}{8\bar{\Theta}}\left(\frac{z}{L}\right)^{5/3}\left[\left(1-\bar{\Theta}\right)^{8/3}-\left(1-\bar{\Theta}\frac{z}{L}\right)^{8/3}\right]\right\} \\
&= A(H,h_0)\exp\left\{-\frac{3}{4\bar{\Theta}}\left(\frac{\kappa}{\kappa_x}\right)^{5/3}\xi^{5/3}\left[\left(1-\bar{\Theta}\xi\right)^{5/3}-\left(1-\bar{\Theta}\right)^{8/3}\right]\right\}
\end{aligned}
\tag{193}
$$

By inserting the spatial filter function and using the same approach as employed in the spherical wave case,

$$
\begin{aligned}
\sigma_{\ln x}^2 &= 8\pi^2L^2A(H,h_0).033\sec(\zeta)A\int_{h_0}^H C_n^2(h)\xi^2\left(1-\bar{\Theta}\xi\right)^2\int_0^\infty\kappa^{4/3} \\
&\times\exp\left\{-\frac{3}{4\bar{\Theta}}\left(\frac{\kappa}{\kappa_x}\right)^{5/3}\xi^{5/3}\left[\left(1-\bar{\Theta}\xi\right)^{5/3}-\left(1-\bar{\Theta}\right)^{8/3}\right]\right\}d\kappa dh \\
&= 1.04A(H,h_0)\left(H-h_0\right)^2\sec^3(\zeta)\kappa_x{}^{7/3}\mu_6
\end{aligned}
\tag{194}
$$

where μ_6 is

$$
\mu_6 = \bar{\Theta}^{7/5}\int_{h_0}^H\frac{C_n^2(h)\xi^{-1/3}\left(1-\bar{\Theta}\xi\right)^2}{\left[\left(1-\bar{\Theta}\xi\right)^{5/3}-\left(1-\bar{\Theta}\right)^{8/3}\right]^{7/5}}dh\,. \tag{195}
$$

By substituting for weak scintillation, (194) yields

$$
\begin{aligned}
\sigma_{\ln y}^2 &\approx 1.56k^{7/6}\left(H-h_0\right)^{5/6}B(H,h_0)\eta_y^{-5/6}\sec^{11/6}(\zeta)\mu_0 \\
&= 0.695B(H,h_0)\eta_y^{-5/6}\frac{\mu_0}{\mu_3}\sigma_2^2
\end{aligned}
\tag{196}
$$

In order to find the weighting constant, A, the horizontal path equivalent of μ_6 is needed. When C_n^2 is constant, μ_6 reduces to [5]

$$\mu_{6,horizontal} = \bar{\Theta}^{7/5} \int_0^1 \frac{\xi^{-1/3}\left(1-\bar{\Theta}\xi\right)^2}{\left[\left(1-\bar{\Theta}\xi\right)^{5/3} - \left(1-\bar{\Theta}\right)^{8/3}\right]^{7/5}} d\xi \approx 1.55\bar{\Theta}^2 - 0.14\bar{\Theta} + 0.65\,, \qquad (197)$$

where the quadratic approximation is at least 91% accurate over the range of Θ from zero to one. Solving for A yields

$$A\left(H, h_0\right) = 4.53\left(1.55\bar{\Theta}^2 - 0.14\bar{\Theta} + 0.65\right)\frac{\mu_3}{\mu_6}\,. \qquad (198)$$

The same method for finding the non-dimensional constants as in previous sections is used,

$$\frac{1}{\eta_x} = \left(1.55\bar{\Theta}^2 - 0.14\bar{\Theta} + 0.65\right)^{6/7}\left[3.46\left(\frac{\sigma_2}{\sigma_B}\right)^{12/7} + 2.15\left(\frac{\mu_3}{\mu_6}\right)^{6/7}\left(\frac{\mu_0}{\mu_3}\right)^{6/5}\sigma_B^{12/5}\right] \qquad (199)$$

$$\eta_y = 8.91\left[\left(\frac{\sigma_2}{\sigma_B}\right)^{12/5} + 0.69\sigma_2^{12/5}\right]. \qquad (200)$$

Inserting these cutoffs into the large-scale and small-scale scintillation indices yield

$$\begin{aligned}\sigma_I^2\left(L\right) &= \exp\left[\sigma_{\ln x}^2 + \sigma_{\ln y}^2\right] - 1 \\ &= \exp\left[\frac{0.49\sigma_B^2}{\left[\left(\frac{\sigma_2}{\sigma_B}\right)^{12/7} + 0.62\left(\frac{\mu_3}{\mu_6}\right)^{6/7}\left(\frac{\mu_0}{\mu_3}\right)^{6/5}\sigma_B^{12/5}\right]^{7/6}} + \frac{0.51\sigma_B^2}{\left(1+0.69\sigma_B^{12/5}\right)^{5/6}}\right] - 1, \quad 0 \le \sigma_B^2 < \infty\end{aligned}\,. \qquad (201)$$

In the *effective* horizontal case, a suitable approximation for (172) was used, which allowed for there to be a more direct relation to all the previous *effective* Kolmogorov cases. Due to the comparatively wide variation of the large-scale scintillation term's denominator, the same parity

is not possible. Combining the longitudinal component with the radial component results in the *effective* scintillation index for a Gaussian beam wave along a slant path,

$$\sigma_I^2(L) = 14.508\mu_1 k^{7/6}\Lambda_e^{5/6}(H-h_0)^{5/6}\sec^{11/6}(\zeta)\frac{r^2}{W_e^2} + \exp\left[\frac{0.49\sigma_B^2}{\left[\left(\frac{\sigma_2}{\sigma_B}\right)^{12/7} + 0.62\left(\frac{\mu_3}{\mu_6}\right)^{6/7}\left(\frac{\mu_0}{\mu_3}\right)^{6/5}\sigma_B^{12/5}\right]^{7/6}} + \frac{0.51\sigma_B^2}{\left(1+0.69\sigma_B^{12/5}\right)^{5/6}}\right] - 1 . \quad (202)$$

A comparison between the weak and *effective* results is displayed in Figures 8. One notices that when comparing only the longitudinal components, the general trend of weak and *effective* results separating from one another occurs when optical turbulence exceeds the weak regime. For slant path scenarios, this is dependent on multiple parameters; Figure 8 uses the zenith angle as a variable with all others fixed. Depending on starting altitude, wavelength, and total height, the separation between the two cases will start at a lower or higher angle.

When comparing the total scintillation index for the standard and *effective* cases, one notices that both results go well above the y-axis. While the standard radial component becomes unbounded, the *effective* radial result mirrors its standard counterpart until it is very close to its horizontal limit, i.e., when the zenith angle is very close to 90 degrees. This shows that one does not gain any insight by using an *effective* beam parameter approach for the radial component along a slant path.

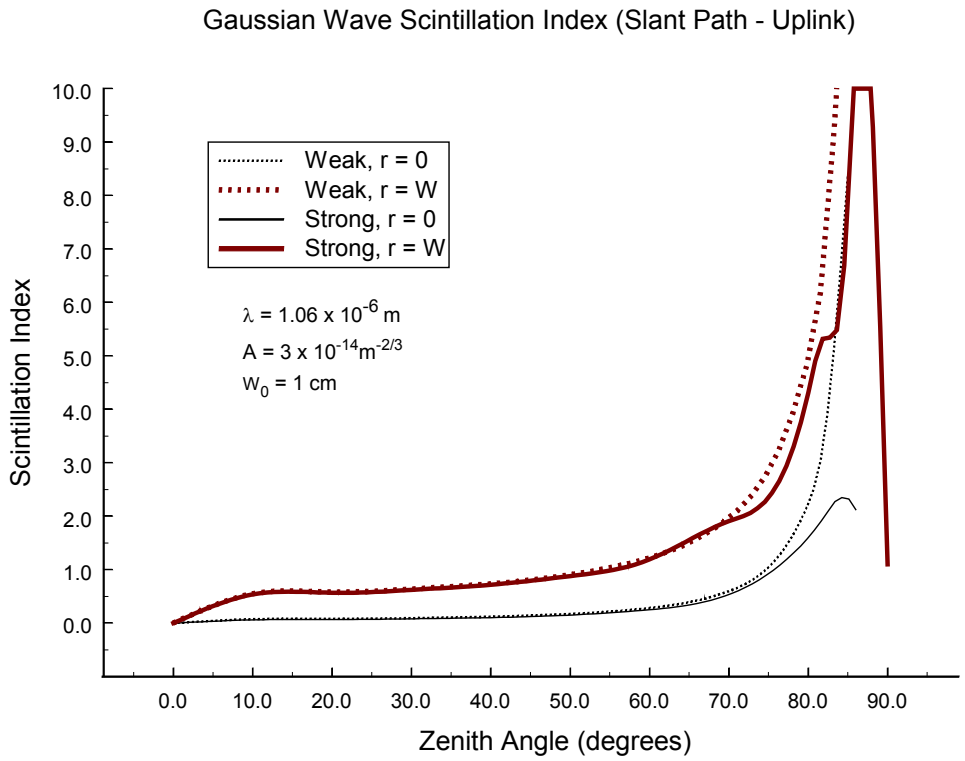

Figure 8: Comparison of weak (186) versus *effective* (202) Gaussian wave scintillation for a collimated beam along a slant path.

In Figure 2, a general roadmap that showed the order of derivations was given. The double-sided arrows were used since the results shown build off of one another. For example, taking any Gaussian beam wave result and setting $\Theta = 0$ and $\Lambda = 0$ would yield the respective spherical wave result. This is apparent in Figure 9 by plotting the *effective* beam index (202) with respect to initial beam size, W_0. As W_0 approaches zero, it becomes a point source, also known as a spherical wave. As W_0 goes to infinity, the beam becomes an unbounded plane wave. The closer W_0 reaches one of these extremes, the closer the Gaussian beam index will mirror the plane or spherical cases.

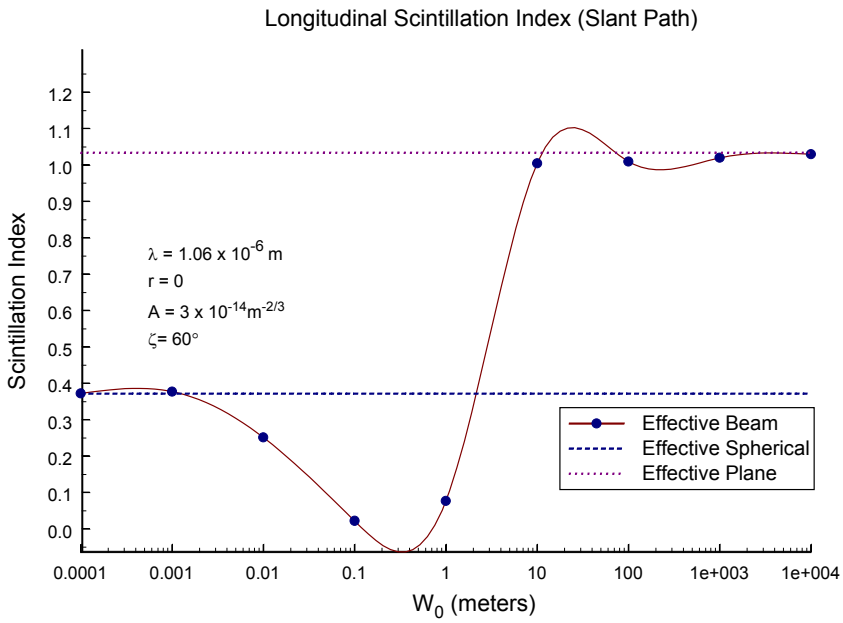

Figure 9: Comparison of uplink *effective* longitudinal scintillation by varying initial beam size.

In Figure 10, the spherical and Gaussian beam *effective* longitudinal scintillation index with respect to varying zenith angle for two different initial beam spot sizes are compared. As expected, the spherical and beam cases are similar when both W_0 and zenith angle are small. However, when strong fluctuation conditions are present, the spherical wave index will underpredict when compared to the Gaussian beam index. In addition, when W_0 is fairly large, the spherical index will overpredict. This is similar behavior that occurs in the scintillation index for a horizontal path.

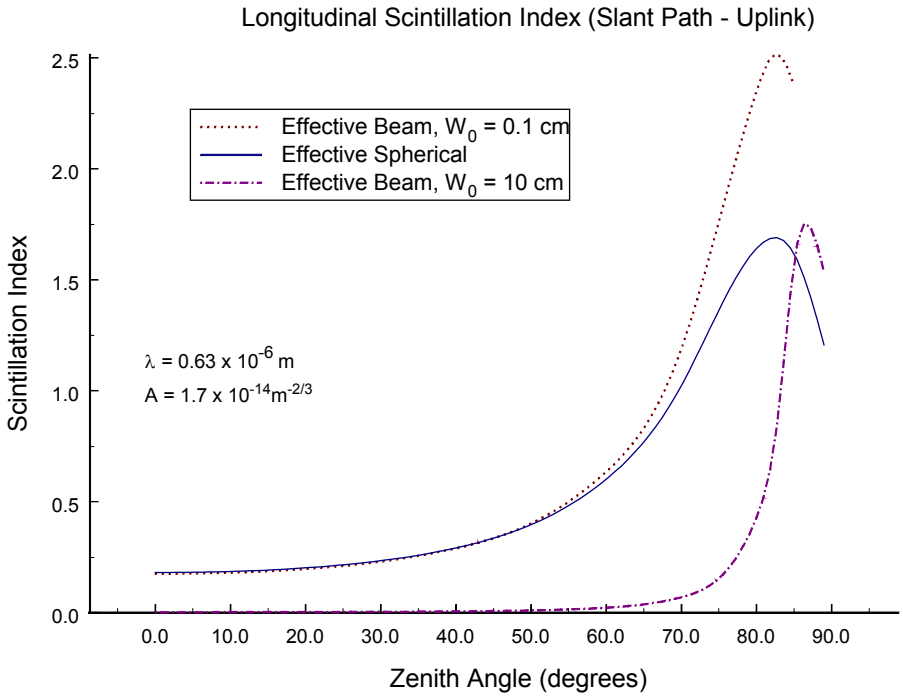

Figure 10: Comparison of uplink *effective* longitudinal scintillation by varying initial beam size.

CHAPTER 8: CONCLUSION

We have developed the theory for the scintillation index of a Gaussian beam wave along a slant path for all regimes of turbulence. We were able to develop a scintillation index that reduces to previously derived results. This theory is usable for uplink propagation paths for satellite communication systems, giving more precise results than its spherical counterpart. In both the spherical and Gaussian beam cases, the modified theory predicts smaller values in high zenith angles than the weak theory, which increases without bound.

Similar to the Gaussian beam scintillation index previously derived for horizontal path, the *effective* index for a Gaussian beam along a slant path captures an optical beam's behavior than its spherical counterpart, particularly when W_0 is large or when the beam is traveling along the horizon.

LIST OF REFERENCES

[1] Andrews , L.C. and Phillips, R.L. (1998). Laser Beam Propagation through Random Media. Bellingham WA: SPIE Optical Engineering Press.

[2] Andrews, L.C., Phillips, R.L. and Hopen, C.Y. (2001). Laser Beam Scintillation with Applications. Bellingham, WA: SPIE Optical Engineering Press.

[3] Andrews, L.C., Phillips, R.L. and Hopen, C.Y., "Scintillation Model for a Satellite Communication Link at Large Zenith Angles," *Opt. Eng.,* **39**, 3272-3280 (2000).

[4] Andrews, L.C., Phillips, R.L., Hopen, C.Y., and Al-Habash, M.A. , "Theory of Optical Scintillation," *J. Opt. Soc. Am. A*, **18**, 1417-1429 (1999).

[5] Thomas, F. E. and Young, C. Y., "Scintillation in Moderate to Strong Optical Turbulence along a Slant Path," *Proc. SPIE*, **5793**, 237-248 (2005).

[6] Young, C Y., Masino, A. J., and Thomas, F. E., "Phase Fluctuations in Moderate to Strong Turbulence," *Proc SPIE*, **4976**, 141-148 (2003).